JOURNAL OF PETROLOGY | VOLUME 43 | NUMBER 10 | PAGES 1787–1814 | 2002

The Substitution of Al and F in Titanite at High Pressure and Temperature: Experimental Constraints on Phase Relations and Solid Solution Properties

PETER TROPPER[1,2]*, CRAIG E. MANNING[2] AND ERIC J. ESSENE[1]

[1]DEPARTMENT OF GEOLOGICAL SCIENCES, UNIVERSITY OF MICHIGAN, 2534 C. C. LITTLE BUILDING, ANN ARBOR, MI 48109-1063, USA

[2]DEPARTMENT OF EARTH AND SPACE SCIENCES, GEOLOGY BUILDING, UNIVERSITY OF CALIFORNIA AT LOS ANGELES, LOS ANGELES, CA 90095-1567, USA

RECEIVED JULY 10, 2001; REVISED TYPESCRIPT ACCEPTED MARCH 26, 2002

Experimental studies were carried out to evaluate phase relations involving titanite–F–Al-titanite solid solution in the system $CaSiO_3$–Al_2SiO_5–TiO_2–CaF_2. The experiments were conducted at 900–1000°C and 1·1–4·0 GPa. The average F/Al ratio in titanite solid solution in the experimental run products is 1·01 ± 0·06, and X_{Al} ranges from 0·33 ± 0·02 to 0·91 ± 0·05, consistent with the substitution $[TiO^{2+}]_{-1}[AlF^{2+}]_1$. Analysis of the phase relations indicates that titanite solid solutions coexisting with rutile are always low in X_{Al}, whereas the maximum X_{Al} of titanite solid solution occurs with fluorite and either anorthite or Al_2SiO_5. Reaction displacement experiments were performed by adding fluorite to the assemblage anorthite + rutile = titanite + kyanite. The reaction shifts from 1·60 GPa to 1·15 ± 0·05 GPa at 900°C, from 1·79 GPa to 1·375 ± 0·025 GPa at 1000°C, and from 1·98 GPa to 1·575 ± 0·025 GPa at 1100°C. The data show that the activity of $CaTiSiO_4O$ is very close to the ideal molecular activity model (X_{Ti}) at 1100°C, but shows a negative deviation at 1000°C and 900°C. The results constrain $\Delta G°_{f,298·15}$ of $CaAlSiO_4F$ to be −2595 ± 3 kJ/mol and $S°_{298·15}$ to be in the range of 105·2–109·6 J/mol K, which in turn can be used to calculate petrogenetic grids involving titanite solid solutions in the system $CaTiSiO_4O$–$CaAlSiO_4F$.

KEY WORDS: *F–Al-titanite; thermodynamic data; TARK; fluorite; reaction displacement*

INTRODUCTION

Geological background

Titanite is a common accessory mineral in mafic, pelitic and granitic rocks from many geological environments (Higgins & Ribbe, 1976; Ribbe, 1982; Enami *et al.*, 1993). Titanite may deviate significantly from its ideal composition by the substitution Al and F for Ti and O (Hollabaugh, 1980; Franz & Spear, 1985; Bernau *et al.*, 1986; Fehr, 1991; Oberti *et al.*, 1991; Carswell *et al.*, 1996). The Al + OH ⇔ Ti + O substitution leads to the Al–OH end-member vuagnatite $CaAlSiO_4(OH)$, which has a different structure from titanite (McNear *et al.*, 1976) and is typical of low-temperature geological environments (Enami *et al.*, 1993). By contrast, the F–Al substitution is isostructural and is common at high metamorphic temperatures (>500–600°C) and pressures. For example, up to 55 mol % F–Al substitution has been reported from high- and ultra-high-pressure metamorphic rocks (Franz & Spear, 1985; Sobolev & Shatsky, 1991; Carswell *et al.*, 1996). The common association of F–Al-rich titanites with high-pressure environments has led to the suggestion that equilibria involving titanite solid solution may be useful for constraining pressure, temperature and/or F_2 fugacity during metamorphism (Smith, 1977; Franz & Spear, 1985; Gibert *et al.*, 1990; Enami *et al.*, 1993; Carswell *et al.*, 1996; Markl & Piazolo, 1999).

*Corresponding author. Present address: Institute of Mineralogy and Petrography, University of Innsbruck, Innrain 52, A-6020 Innsbruck, Austria. E-mail: Peter.Tropper@uibk.ac.at

Despite the importance of the F–Al content of titanite there are few experimental data available with which to evaluate the physical and chemical controls on titanite solid solutions. The F–Al substitution was examined by Smith (1981) and Troitzsch & Ellis (1999). Smith (1981) synthesized titanite with about 50 mol % F–Al titanite substitution at 1000–1200°C and 1·5–3·5 GPa, similar to the upper limit of substitution reported from various natural occurrences. He also found an increase in the F–Al substitution with falling temperature and increasing pressure. Troitzsch & Ellis (1999) synthesized end-member F–Al-titanite at 1100°C and high pressure, and demonstrated complete solid solution in the system $CaTiSiO_4O$–$CaAlSiO_4F$.

In high-pressure rocks, titanite and rutile also form the basis of a set of equilibria useful for the determination of pressure. Specific equilibria discussed by Manning & Bohlen (1991) include

$$3Ca_2Al_3Si_4O_{12} + 5TiO_2 + 2SiO_2 + H_2O = 5CaTiSiO_4O + 2Ca_2Al_3Si_3O_{12}(OH) \quad (1)$$

Grossular + Rutile + Quartz + H_2O = Titanite + Zoisite

$$Ca_2Al_3Si_4O_{12} + 3TiO_2 + SiO_2 = CaTiSiO_4O + Al_2SiO_5 \quad (2)$$

Grossular + Rutile + Quartz/Coesite = Titanite + Kyanite.

Manning & Bohlen (1991) used these reactions to estimate pressures in high-pressure rocks from Scotland and Austria and ultra-high-pressure rocks from Kazakhstan. The successful application of reactions (1) and (2) to thermobarometry illustrates the utility of titanite-bearing equilibria in petrology. However, the accuracy of the results depends on understanding the subsolidus properties of titanite solid solutions and relevant phase equilibria. We focus here on phase relations involving F–Al-titanite.

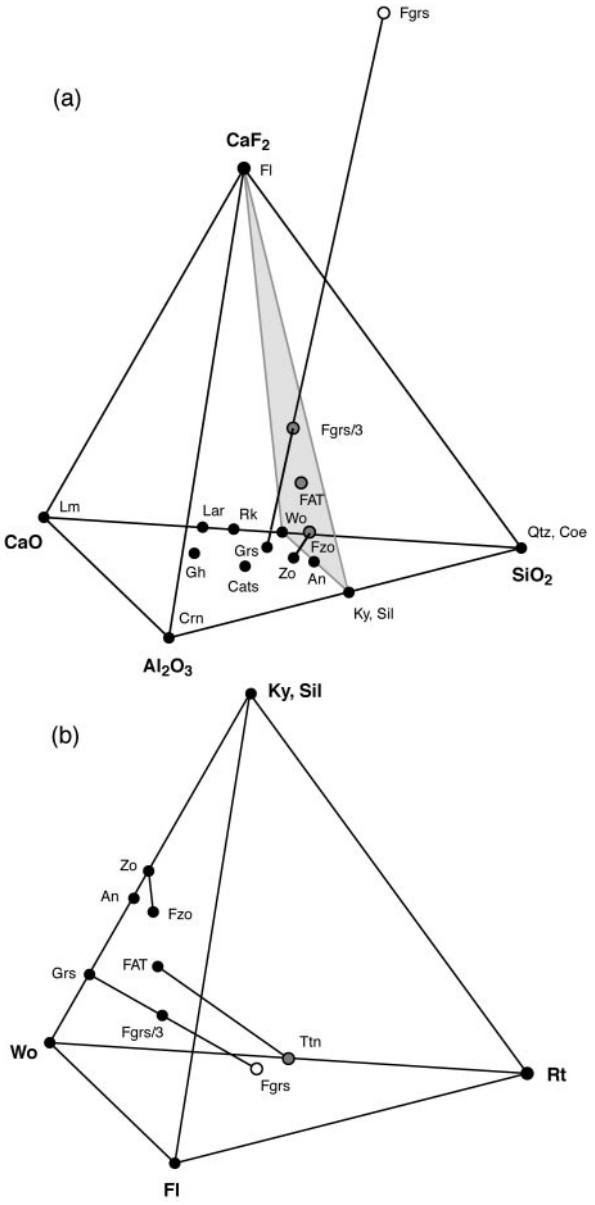

Fig. 1. (a) CaO–CaF_2–Al_2O_3–SiO_2 quaternary. Perovskite-type phases ($CaTiO_3$ and intermediate $CaTi_xSi_{1-x}O3$; e.g. Leinenweber *et al.*, 1997) are omitted. The shaded area marks the triangle wollastonite–kyanite–fluorite and contains end-member F–Al-titanite (FAT), F-bearing zoisite (Fzo) and an intermediate F-grossular–grossular solid solution, Fgrs/3; ●, minerals on basal CaO–Al_2O_3–SiO_2 plane; gray circles, F-bearing minerals in wollastonite–Al_2SiO_5–fluorite plane; ○, F-grossular (Fgr), which projects outside the quaternary volume. Tie lines link relevant solid solutions. (b) Wollastonite–rutile–kyanite–fluorite quaternary illustrating the phase relations among anorthite–kyanite–titanite–rutile–F–Al-titanite (FAT)–fluorite; ●, minerals on or projecting onto wollastonite–Al_2SiO_5–fluorite plane; gray circles, Ti-bearing compositions; ○, F-grossular (Fgr), which projects outside the quaternary volume. Tie lines link relevant solid solutions. All mineral abbreviations according to Kretz (1983) except: Cats, Ca-Tschermaks; Coe, coesite; FAT, F–Al-titanite; Fgrs and Fgrs/3, F-grossular and F-grossular–grossular solid solution; Fzo, F-zoisite; Lar, larnite; Lm, lime; Rk, rankinite.

Preliminary analysis of phase relations

Examination of the compositional space relevant to F–Al-titanite solid solution provides guidance for the design and interpretation of the present experiments, and for comparison with previous work. Figure 1 illustrates that a variety of F-bearing phases must be considered. In the basal plane of the quaternary CaO–Al_2O_3–SiO_2–CaF_2 (Fig. 1a), anhydrous, high-temperature Ca–Al silicates are coplanar (zoisite is projected into this space for comparison with its fluorian analogue). Relevant F-bearing phases, which plot above the basal plane in Fig. 1a, include in order of increasing relative CaF_2 content, hypothetical F-zoisite ($Ca_2Al_3Si_3O_{12}F$), F–Al-titanite

($CaAlSiO_4F$), and the hypothetical F-grossular end-member ($Ca_3Al_2\square_3F_{12}$). Also shown are the intermediate compositions on the grossular–F-grossular join, $Ca_3Al_2Si_2\square O_8F_4$, which is collinear with anorthite and fluorite, and $Ca_3Al_2Si_{1.5}\square_{1.5}O_6F_6$, which is coplanar with fluorite, quartz and kyanite.

Mapping the coordinate system in Fig. 1a to $CaSiO_3$–Al_2SiO_5–CaF_2 allows addition of TiO_2 (Fig. 1b) and illustrates the positions of titanite–F–Al-titanite solid solution. Anhydrous F-zoisite or F-grossular have not been reported from nature or experiments. Fluorian zoisite was identified by Troitzsch & Ellis (1999) in their F–Al-titanite synthesis experiments, but they determined that it contained significant hydroxyl. Fluorian grossular–andradite solid solutions occur naturally (e.g. Valley *et al.*, 1983; Manning & Bird, 1990), but stoichimetric considerations imply significant OH as well. The extent to which hydroxyl substitution is required to stabilize these F-bearing phases is unknown; nevertheless, the possibility of F substitution along these trajectories must be considered, especially in anhydrous experimental systems at high *T* and *P*.

The mechanisms of F substitution differ in zoisite, grossular and titanite. In zoisite, a simple $[OH^-]_{-1}[F^-]_1$ exchange operates; in F-grossular, F substitution is coupled to Si vacancies via $[SiO_4^{4-}]_{-1}[\square F_4^{4-}]_1$; and the exchange vector for the titanite solid solution is $[TiO^{2+}]_{-1}[AlF^{2+}]_1$. Thus, in addition to *P* and *T*, the chemical potentials of the thermodynamic components F_2, SiO_2, H_2O, Al_2O_3 and TiO_2 must all be considered in evaluating phase equilibria involving F–Al-titanite solid solution.

Because of the many variables that might control phase assemblages and compositions, it is useful to identify that appropriate portion of compositional space that is most geologically relevant. Figure 1a shows that phases on the fluorite–wollastonite–kyanite plane are silica-rich and are, therefore, most likely to be associated with quartz in natural systems. Thus, we focused our efforts on the compositional region encompassed by the phases wollastonite–kyanite–rutile–titanite–fluorite; that is, the region depicted in Fig. 1b. Additional relevant phases within the bounding compositions are F-zoisite, F–Al-titanite, and F-grossular. Although the grossular–F-grossular solid solution intersects the anorthite–fluorite join at $Ca_3Al_2Si_2\square O_8F_4$, we anticipate that this substitution is minimized when the investigated bulk compositions are at or near quartz saturation.

Ignoring F-zoisite, which is unknown in nature, there are two reactions involving F–Al-titanite (Fig. 1b):

$$CaAl_2Si_2O_8 + CaF_2 = 2CaAlSiO_4F \quad (3)$$

Anorthite + Fluorite = F–Al-Titanite

$$CaTiSiO_4O + Al_2SiO_5 + CaF_2 = 2CaAlSiO_4F + TiO_2 \quad (4)$$

Titanite + Kyanite + Fluorite = F–Al-Titanite + Rutile.

Consideration of the geometric relations in Fig. 1b indicates that is there is only one other possible reaction among these phases,

$$CaTiSiO_4O + Al_2SiO_5 = CaAl_2Si_2O_8 + TiO_2 \quad (5)$$

Titanite + Kyanite = Anorthite + Rutile

which was experimentally investigated by Manning & Bohlen (1991). We use the acronyms AFT, TAFT and TARK for reactions (3), (4) and (5), respectively.

Relative stabilities in *P*–*T* space can be predicted using estimated properties of Al–F-titanite. The volume ($V°_{298·15}$) of synthetic Al–F-titanite was determined by Troitzsch & Ellis (1999) to be 344·11 Å^3 or 51·805 cm^3/mol (Troitzsch & Ellis, 1999). This is ~7% smaller than the reported volume of end-member titanite $CaTiSiO_4O$, which varies from 55·74 cm^3/mol (Robie & Hemingway, 1995) to 55·64 cm^3/mol (Xirouchakis & Lindsley, 1998). The volume is also slightly lower than the 52·5 cm^3/mol that was predicted for pure $CaAlSiO_4F$ by Oberti *et al.* (1991) by extrapolation of volume data from natural Al–F-bearing titanites.

The entropy ($S°_{298·15}$) is estimated here by additive techniques (Robinson & Haas, 1983). Two estimates are made. The first, based on a reaction among orthosilicates,

$$2CaAlSiO_4F = Al_2SiO_4F_2 + 2CaMgSiO_4 - Mg_2SiO_4 \quad (6)$$

Al–F-Titanite = Topaz + Monticellite − Forsterite

yields $S°_{298·15}$ for Al–F-titanite of 105·2 J/mol K. The second estimate used the reaction among oxides and fluorides, where the data for the oxides were taken from Holland (1989) and those for fluorite were taken from Robie & Hemigway (1995),

$$2CaAlSiO_4F = CaF_2 + CaO + Al_2O_3 + 2SiO_2 \quad (7)$$

Al–F-Titanite = Fluorite + Lime + Corundum + Quartz

and gives $S°_{298·15}$ = 109·6 J/mol K after applying a volume correction. These entropy estimates of 105–110 J/mol K are significantly lower than the entropy of titanite, which has been inferred to range from 129·2 J/mol K (Robie & Hemingway, 1995) to 131·2 J/mol K (Holland & Powell, 1998), but similar to the value of 107·8 J/mol K estimated by Xirouchakis & Lindsley (1998). Their $S°_{298·15}$ for titanite is too low to be consistent with phase equilibrium constraints of Manning & Bohlen (1991).

The slopes of reactions (3)–(5) were calculated using our estimated ranges of $S°_{298·15}$ and $V°_{298·15}$ for F–Al-titanite, along with data for the other minerals from Robie & Hemingway (1995). The calculations yield dP/dT for reaction (3) ranging from 26·9 to 28·9 bar/°C. The Clapeyron slope of the TAFT reaction (4) is much steeper and ranges from 55·5 to 123·5 bar/°C. The estimate for reaction (5) is 17·2–19·2 bar/°C, similar to the Clapeyron slopes of 20·5–23·5 bar/°C obtained by Manning & Bohlen (1991). Our calculations therefore suggest that the AFT equilibrium (3) has a slightly steeper slope than equilibrium (5) suggesting that the two reactions intersect, with reaction (3) stable at higher pressures at high temperatures.

Scope of the study

The relative shifts of the three equilibria (3)–(5) as a consequence of titanite solid solution are unknown. Quantitative analysis of these phase relations, and related solution energetics and thermodynamic properties, require experimental studies of appropriate equilibria and bulk compositions. The first part of this study involves the assessment of conditions of F–Al-titanite stability and examination of reaction (4) to explore its possible utility for application to metamorphic phase equilibria. The second part of this study focuses on the thermodynamics of mixing in $CaTiSiO_4O$–$CaAlSiO_4F$ solid solutions and the derivation of thermodynamic properties of $CaAlSiO_4F$.

METHODS

Starting materials

Natural and synthetic minerals were used as starting materials. Natural kyanite from Brazil (0·15 wt % Fe_2O_3, Bohlen *et al.*, 1991) was boiled in concentrated HF for ~3·5 h to dissolve minor adhering sheet silicate grains and then fired at 950°C overnight. We used synthetic titanite from Manning & Bohlen (1991). Anorthite was synthesized from high-grade (99·99% pure) SiO_2, Al_2O_3 and $CaCO_3$. The mixture was decarbonated at 1000°C overnight and then melted in a Pt crucible at 1600°C for 30 min. The quenched glass was ground and then crystallized at 1400°C over a period of 2 days, with repeated grinding. Rutile was synthesized by firing TiO_2 at 1000°C over a period of 3 days, with repeated grinding. Synthetic fluorite (Fisher Co.) and natural fluorite from the microprobe standard collection of the Electron Microprobe Analysis Laboratory, University of Michigan, were used. Anorthite, titanite and kyanite were analyzed by electron microprobe (EMP) analyses and X-ray powder diffraction to verify their purity. X-ray powder diffraction confirmed the absence of additional phases in the rutile and natural and synthetic fluorite.

Run procedures

All experiments were conducted in an end-loaded piston–cylinder apparatus at UCLA similar to that described by Boyd & England (1960) with 25·4 mm (1 inch) diameter furnace assemblies and pistons for runs below 2·0 GPa; at higher pressures, 12·7 mm (1/2 inch) furnace assemblies and pistons were used. The furnace assembly is primarily made of graphite, NaCl and MgO (Bohlen, 1984; Manning & Boettcher, 1994). The furnace assembly for high-temperature runs contained a Pyrex sleeve between the graphite furnace and the salt cell to prevent the penetration of salt melts into the graphite furnace (Boettcher *et al.*, 1981; Manning & Boettcher, 1994).

Stoichiometric mixtures of the starting materials were sealed in a welded $Ag_{80}Pd_{20}$ capsule with 2 mm diameter. The capsule was placed horizontally in the graphite furnace and packed in boron nitride (BN) to reduce temperature gradients. A piece of Pt foil was placed on top of the capsule to prevent puncture by the thermocouple. Temperature was measured with a type S ($Pt/Pt_{90}Rh_{10}$) thermocouple, with a precision estimated to be ± 3°C, and pressures was monitored using a Heise gauge having a precision of about $\pm 0·01$ GPa.

The piston-in method (Johannes *et al.*, 1971) was used for every experiment. First, a pressure of about two-thirds of that to be maintained during the run was applied to the furnace assembly. The temperature was then raised to the desired temperature of the run over a period of ~10 min and finally the pressure was increased to the desired value. In the high-temperature runs, pressure was increased to about 0·3–0·5 GPa and then the temperature was raised to 700°C to ensure ductile behavior of the Pyrex sleeve. Afterwards, the pressure was increased to ~0·2 GPa below the desired value and then the temperature was raised to the final value.

Analytical techniques

X-ray powder diffraction was conducted using a conventional Norelco–Philips vertical diffractometer with variable slit geometry. All run products were analyzed by scanning electron microscopy (SEM) and EMP analysis. Electron microprobe analyses were obtained with the Cameca CAMEBAX EMP at the Electron Microbeam Analyses Laboratory (EMAL) of the University of Michigan. Additional EMP analyses were obtained with the Cameca CAMEBAX EMP at UCLA. Analyses were obtained at 15 kV and 10 nA beam current with a point beam. Natural and synthetic mineral standards included Topaz Mt. topaz (F), synthetic rutile (Ti) and natural

Table 1: Piston–cylinder experiment conditions and results

(Series) starting phases	Mole ratios	Run	*P* (GPa)	*T* (°C)	Time (h)	*X*(Al)	Experimental products observed
(A) An + Fl*	1:2	246	2·0	1000	46	—	F-Zo + An + Fl + Qtz
(A) An + Fl	1:2	228	2·0	1000	71	—	F-Zo + An + Fl + Qtz
(B) An + Ttn seeds + Fl*	1:0·046:2	247	2·0	1000	46	0·91 ± 0·05	FAT + F-Zo + An + Fl + Qtz
(C1) An + Ttn + Fl	1:1:3	231	2·0	1000	79	0·77 ± 0·04	FAT + F-Zo + An + Fl + Qtz
(C2) An + Ttn + Fl	1:0·36:1	26	2·0	1000	36	0·82 ± 0·02	FAT + F-Zo + An + Fl + Qtz
(D1) An + Ky + Ttn + Fl	1:1:1:3·6	232	2·0	1000	79	0·89 ± 0·05	FAT + F-Zo + Ky + An + Fl + Qtz
(D2) An + Ky + Ttn + Fl	1:0·05:0·05:1	79	2·0	1000	80	0·89 ± 0·03	FAT + F-Zo + Ky + An + Fl + Qtz
(D3) An + Ky + Ttn + Fl	1:0·05:1:1·5	80	2·0	1000	80	0·90 ± 0·03	FAT + F-Zo + Ky + An + Fl + Qtz
(D4) An + Ky + Ttn + Fl	1:0·3:1:1·5	81	2·0	1000	80	0·87 ± 0·02	FAT + F-Zo + Ky + An + Fl + Qtz
(E) An + Qtz + Ttn + Fl	1:1:0·5:2·6	233	2·0	1000	79	0·71 ± 0·05	FAT + An + Fl + Qtz
(F) Ttn + Rt + Ky + Fl	1:1:1:1·5	226	2·0	1000	114	0·51 ± 0·00	FAT + Rt + Ky + Qtz + Cor + Fl + melt
(F) Ttn + Rt + Ky + Fl	1:1:1:1·5	20	2·0	900	48	0·54 ± 0·04	FAT + Rt + Qtz + Ky + Fl
(F) Ttn + Rt + Ky + Fl	1:1:1:1·5	18	2·0	1000	24	0·52 ± 0·01	FAT + Rt + Qtz + Ky + Fl
(F) Ttn + Rt + Ky + Fl	1:1:1:1·5	46	1·1	1000	46	0·33 ± 0·05	FAT + Rt + Qtz + An + Fl
(F) Ttn + Rt + Ky + Fl	1:1:1:1·5	257	1·5	1000	39	0·47 ± 0·03	FAT + Rt + Qtz + Ky + Fl
(F) Ttn + Rt + Ky + Fl	1:1:1:1·5	217	3·0	1000	94	0·56 ± 0·02	FAT + Rt + Qtz + Ky + Fl
(F) Ttn + Rt + Ky + Fl	1:1:1:1·5	218	4·0	1000	117	0·55 ± 0·03	FAT + Rt + Qtz + Ky + Fl
(F) Ttn + Rt + Ky + Fl	1:1:1:1·5	220	2·0	900	118	0·55 ± 0·03	FAT + Rt + Qtz + Ky + Fl
(F) Ttn + Rt + Ky + Fl	1:1:1:1·5	256	1·3	1100	16	0·43 ± 0·01	FAT + Rt + Qtz + An + Fl
(F) Ttn + Rt + Ky + Fl	1:1:1:1·5	259	1·7	1100	24	0·49 ± 0·01	FAT + Rt + Qtz + Ky + Fl
(F) Ttn + Rt + Ky + Fl	1:1:1:1·5	187	2·0	1100	50	0·51 ± 0·01	FAT + Rt + Qtz + Ky + Fl
(F) Ttn + Rt + Ky + Fl	1:1:1:1·5	261	3·0	1100	25	0·53 ± 0·03	FAT + Rt + Qtz + Ky + Fl
(F) Ttn + Rt + Ky + Fl	1:1:1:1·5	265	4·0	1100	36	0·57 ± 0·01	FAT + Rt + Qtz + Ky + Fl
(G) Ttn + 3Rt + Ky + Fl	1:3:1:2	227	2·0	1000	114	0·51 ± 0·02	FAT + Rt + Ky + Qtz + Fl
(H) Ttn + Ky + An + Rt + Fl	1:1:1:1:3·6	262	1·1	900	73	0·42 ± 0·03	FAT + Rt + Qtz + Ky + An + Fl
(H) Ttn + Ky + An + Rt + Fl	1:1:1:1:3·6	251	1·2	900	66	0·48 ± 0·04	FAT + Rt + Qtz + Ky + An + Fl
(H) Ttn + Ky + An + Rt + Fl	1:1:1:1:3·6	238	1·2	1000	72	0·41 ± 0·05	FAT + Rt + Qtz + An + Fl
(H) Ttn + Ky + An + Rt + Fl	1:1:1:1:3·6	239	1·3	1000	82	0·50 ± 0·03	FAT + Rt + Qtz + Ky + An + Fl
(H) Ttn + Ky + An + Rt + Fl	1:1:1:1:3·6	269	1·35	1000	75	0·51 ± 0·03	FAT + Rt + Qtz + Ky + An + Fl
(H) Ttn + Ky + An + Rt + Fl	1:1:1:1:3·6	249	1·35	1000	43	0·48 ± 0·05	FAT + Rt + Qtz + Ky + An + Fl
(H) Ttn + Ky + An + Rt + Fl	1:1:1:1:3·6	234	1·4	1000	72	0·53 ± 0·02	FAT + Rt + Qtz + Ky + An + Fl
(H) Ttn + Ky + An + Rt + Fl	1:1:1:1:3·6	235	1·6	1000	72	0·50 ± 0·02	FAT + Rt + Qtz + Ky + Fl
(H) Ttn + Ky + An + Rt + Fl	1:1:1:1:3·6	237	1·8	1000	75	0·54 ± 0·04	FAT + Rt + Qtz + Ky + Fl
(H) Ttn + Ky + An + Rt + Fl	1:1:1:1:3·6	230	2·0	1000	73	0·51 ± 0·02	FAT + Rt + Qtz + Ky + Fl
(H) Ttn + Ky + An + Rt + Fl	1:1:1:1:3·6	242	1·4	1100	48	0·47 ± 0·02	FAT + Rt + Qtz + An + Fl
(H) Ttn + Ky + An + Rt + Fl	1:1:1:1:3·6	243	1·5	1100	23	0·48 ± 0·03	FAT + Rt + Qtz + An + Fl + Cor
(H) Ttn + Ky + An + Rt + Fl	1:1:1:1:3·6	266	1·55	1100	66	0·49 ± 0·01	FAT + Rt + Qtz + Ky + An + Fl + Cor
(H) Ttn + Ky + An + Rt + Fl	1:1:1:1:3·6	248	1·55	1100	8	0·50 ± 0·04	FAT + Rt + Qtz + Ky + An + Fl
(H) Ttn + Ky + An + Rt + Fl	1:1:1:1:3·6	240	1·6	1100	43	0·51 ± 0·02	FAT + Rt + Qtz + Ky + An + Fl
(H) Ttn + Ky + An + Rt + Fl	1:1:1:1:3·6	245	1·8	1100	6	0·57 ± 0·04	FAT + Rt + Qtz + Ky + Fl + Ca-phase
(H) Ttn + Ky + An + Rt + Fl	1:1:1:1:3·6	236	2·0	1100	55	0·53 ± 0·05	FAT + Rt + Qtz + Ky + Fl

*Experiments where fH_2 was buffered; all abbreviations are according to Kretz (1983) except FAT (F-Al-titanite$_{ss}$) and F-Zo (F-bearing zoisite); An, anorthite; Ky, kyanite; Wo, wollastonite; Gro, grossular; Rt, rutile; Fl, fluorite; Qtz, quartz; Ttn, titanite; Cor, corundum.

Table 2a: Electron microprobe analyses of F–Al-titanite from the experiments with different bulk compositions

Run no. (series):	247 (B)	231 (C1)	26 (C2)	232 (D1)	79 (D2)	80 (D3)	81 (D4)	233 (E)	227 (G)
P (GPa):	2·0	2·0	2·0	2·0	2·0	2·0	2·0	2·0	2·0
T (°C):	1000	1000	1000	1000	1000	1000	1000	1000	1000
n:	6	10	10	9	13	6	7	12	4
SiO_2	33·20(60)	32·54(34)	33·30(45)	32·94(65)	34·07(46)	33·65(34)	33·78(23)	32·13(32)	31·84(14)
TiO_2	3·93(208)	9·95(193)	7·77(90)	4·85(207)	5·09(137)	4·52(140)	5·79(74)	12·38(187)	20·68(79)
Al_2O_3	25·52(140)	21·25(117)	23·25(71)	24·41(136)	25·41(104)	25·75(110)	24·88(58)	19·58(192)	13·73(31)
CaO	31·60(88)	30·95(24)	30·54(38)	31·24(56)	31·04(75)	31·03(24)	31·14(21)	30·22(92)	29·90(14)
F	9·79(105)	7·88(59)	7·91(41)	9·77(63)	8·97(48)	9·31(56)	8·75(22)	7·52(69)	5·42(13)
O=F	4·12(44)	3·32(25)	3·33(17)	4·11(27)	3·78(20)	3·92(24)	3·68(09)	3·17(29)	2·28(06)
Σ	99·91(75)	99·25(44)	99·43(80)	99·09(36)	100·80(69)	100·33(50)	100·66(42)	98·66(40)	99·28(42)
F	0·93(10)	0·77(05)	0·75(04)	0·94(06)	0·83(05)	0·87(04)	0·82(02)	0·74(07)	0·54(01)
Si	1·00	1·00	1·00	1·00	1·00	1·00	1·00	1·00	1·00
Al	0·91(05)	0·77(04)	0·82(02)	0·87(05)	0·88(03)	0·90(03)	0·87(02)	0·72(07)	0·51(01)
Ca	1·02(04)	1·02(01)	0·98(02)	1·02(04)	0·98(03)	0·99(01)	0·99(01)	1·01(03)	1·01(01)
Ti	0·09(05)	0·23(05)	0·18(02)	0·11(05)	0·11(03)	0·10(03)	0·13(02)	0·29(05)	0·49(02)
Σ	3·02(05)	3·02(02)	2·98(02)	3·00(06)	2·97(04)	2·99(01)	2·98(01)	3·02(02)	3·00(01)
X(Al)	0·91(05)	0·77(04)	0·82(02)	0·89(05)	0·89(03)	0·90(03)	0·87(02)	0·71(05)	0·51(02)

The titanite analyses of series F (run 226) are shown in Table 2b and the analyses of series H (run 230) are shown in Table 2c.

Table 2b: Electron microprobe analyses of F–Al-titanite from the experiments with bulk composition (series) F

Run no.:	46	257	226	217	218	220	256	259	187	261	265
P (GPa):	1·1	1·5	2·0	3·0	4·0	2·0	1·3	1·7	2·0	3·0	4·0
T (°C):	1000	1000	1000	1000	1000	900	1100	1100	1100	1100	1100
n:	3	6	7	8	10	3	6	8	11	7	9
SiO_2	30·96(15)	31·26(27)	31·34(14)	31·81(32)	31·53(29)	32·06(19)	31·75(23)	31·55(30)	31·70(27)	31·35(60)	32·53(25)
TiO_2	28·77(227)	23·68(130)	20·66(20)	18·91(100)	18·98(80)	19·21(136)	24·39(47)	22·31(90)	20·94(32)	20·66(193)	18·58(51)
Al_2O_3	8·88(142)	13·19(101)	13·95(10)	15·49(71)	15·67(42)	14·86(74)	11·97(37)	13·54(19)	13·81(18)	14·68(55)	15·41(36)
CaO	29·09(14)	28·94(40)	29·70(18)	29·49(28)	29·44(27)	29·87(12)	29·98(25)	29·64(47)	29·65(23)	29·44(59)	29·19(25)
F	3·47(26)	4·85(16)	5·52(14)	5·77(24)	5·89(28)	5·53(33)	4·48(22)	4·95(13)	5·32(12)	5·48(09)	6·07(22)
O=F	1·46(11)	2·04(07)	2·32(06)	2·43(10)	2·48(12)	2·33(14)	1·89(09)	2·08(05)	2·24(05)	2·31(04)	2·56(09)
Σ	99·70(55)	99·86(25)	98·84(25)	99·03(51)	99·04(33)	99·29(24)	100·68(72)	99·89(37)	99·18(65)	99·29(47)	99·23(36)
F	0·35(03)	0·49(02)	0·56(01)	0·57(02)	0·59(03)	0·55(03)	0·45(02)	0·50(02)	0·53(01)	0·55(01)	0·59(02)
Si	1·00	1·00	1·00	1·00	1·00	1·00	1·00	1·00	1·00	1·00	1·00
Al	0·34(05)	0·50(04)	0·52(00)	0·57(02)	0·59(01)	0·55(02)	0·44(01)	0·51(01)	0·51(01)	0·55(01)	0·56(01)
Ca	1·01(01)	0·99(01)	1·02(01)	0·99(01)	1·00(01)	1·00(00)	1·01(00)	1·01(01)	1·00(01)	1·01(01)	0·96(01)
Ti	0·70(06)	0·60(04)	0·50(01)	0·45(03)	0·45(02)	0·45(03)	0·58(01)	0·53(03)	0·50(01)	0·50(01)	0·43(01)
Σ	3·04(01)	3·06(02)	3·04(01)	3·01(03)	3·04(02)	3·00(01)	3·03(01)	3·04(02)	3·01(01)	3·05(05)	2·95(01)
X(Al)	0·33(05)	0·47(03)	0·51(00)	0·56(02)	0·56(02)	0·55(03)	0·43(01)	0·49(01)	0·51(01)	0·53(03)	0·57(01)

All formulae are normalized to 1 Si; *X*(Al), [Al/(Al + Ti)]; numbers in parentheses are 1σ standard deviations; *n*, number of analyses.

tanzanite (Ca, Al, Si). Fluorine was analyzed on the multilayer crystal OV60 (6 nm *d*-spacing). The counting times were 50 s for F and 30 s for all other elements. Raw data were reduced with a PAP-type correction. The titanites of runs 265, 248 and 249 were analyzed with a JEOL 6310 SEM equipped with a LINK ISIS energy-dispersive system and a MICROSPEC wavelength-dispersive system at the Institute of Mineralogy and Petrology, University of Graz. The analytical conditions were 15 kV and 5 nA sample current. The elements Si, Al, Ca and Ti were analyzed with the energy-dispersive system and the F content was analyzed with the wavelength-dispersive system, because of the lower detection limit of 0·05–0·1 wt % of the wavelength-dispersive system.

RESULTS

Titanite solid solutions were produced with a range of starting assemblages at 900–1100°C and 1·1–4·0 GPa (Table 1). We prepared starting mixtures with 12 molar ratios of fluorite ± anorthite, rutile, kyanite, titanite and quartz (series A–H; Table 1). The run duration was between 23 and 118 h for most experiments, depending on the temperature as shown in Table 1. It is likely that such long durations are conservative, inasmuch as two short runs (run 248, 8 h; run 245, 6 h) yielded sufficient reaction progress to determine the reaction direction.

Equilibrium constraints

Owing to the high temperatures of all experiments (900–1100°C), reaction rates were rapid and the growth of F–Al-rich titanite could easily be observed in the run products. Using the starting assemblage titanite + kyanite + rutile + fluorite, we evaluated equilibration in our experiments in two ways. First, different bulk compositions with varying rutile and fluorite content (series F and G), or varying titanite, kyanite and fluorite content (series D1–D4) were run side by side at the same P, T and time. The compositions of newly grown titanite$_{ss}$ in experiments with mix F (run 226) and mix G (run 227) were identical and yield $X_{Al} = 0{\cdot}51$ as shown in Table 2a and b. The results from the experiments with mixtures D1–D4 also result in the same X_{Al} of 0·87–0·90 in titanite$_{ss}$ (Table 2a). In a second test of equilibrium, experiments at 900 and 1000°C and 2·0 GPa (series F) and experiments at 1000°C and 1·35 GPa and 1100°C and 1·55 GPa (series H) were run for different durations to compare the compositions (X_{Al}) of the newly grown titanite$_{ss}$ as a function of time. In these runs, experiments with mix F (kyanite + rutile + titanite + fluorite) at 900°C yielded statistically indistinguishable X_{Al} of 0·54 ± 0·04 and 0·55 ± 0·03 regardless of whether the run duration was 48 or 118 h (Fig. 2a). Similarly, titanite$_{ss}$ from the experiments at 1000°C with the same assemblage have X_{Al} of 0·52 ± 0·01 and 0·51 ± 0·00 obtained at 24 and 114 h run (Fig. 2b). Two experiments with mixture H were also run with different run durations. The experiment at 1000°C and 1·35 GPa was run for 43 h (run 249) and 75 h (run 269). Both runs yielded similar X_{Al} of 0·48 ± 0·05 and 0·51 ± 0·03. At 1100°C, the experiment at 1·55 GPa was also conducted with different run times. Run 248 and run 266 yielded a

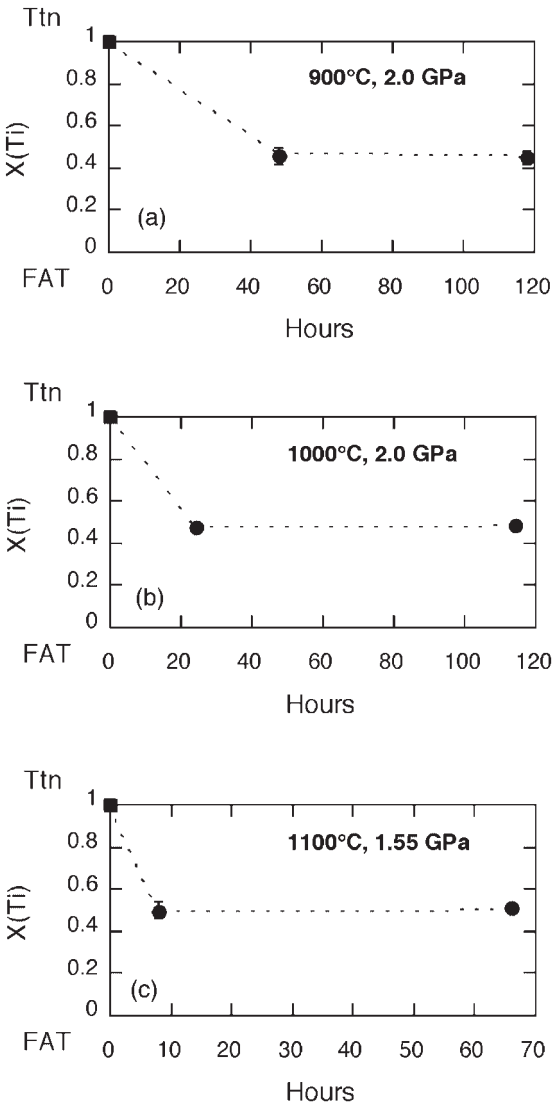

Fig. 2. Plot of X_{Ti} in titanite$_{ss}$ vs time at 2·0 GPa and 900°C (a) and 1000°C (b) and 1·55 GPa and 1100°C (c). The experiments were conducted with the assemblage kyanite + rutile + fluorite + titanite (series F). ●, compositions of the synthetic titanites from the experiments at 24 h (run 18) and 114 h (run 226); ■, composition of the starting titanite. The dashed line indicates the compositional trend. The error bars are one standard deviation (1σ), and are omitted if 1σ is smaller than the symbol.

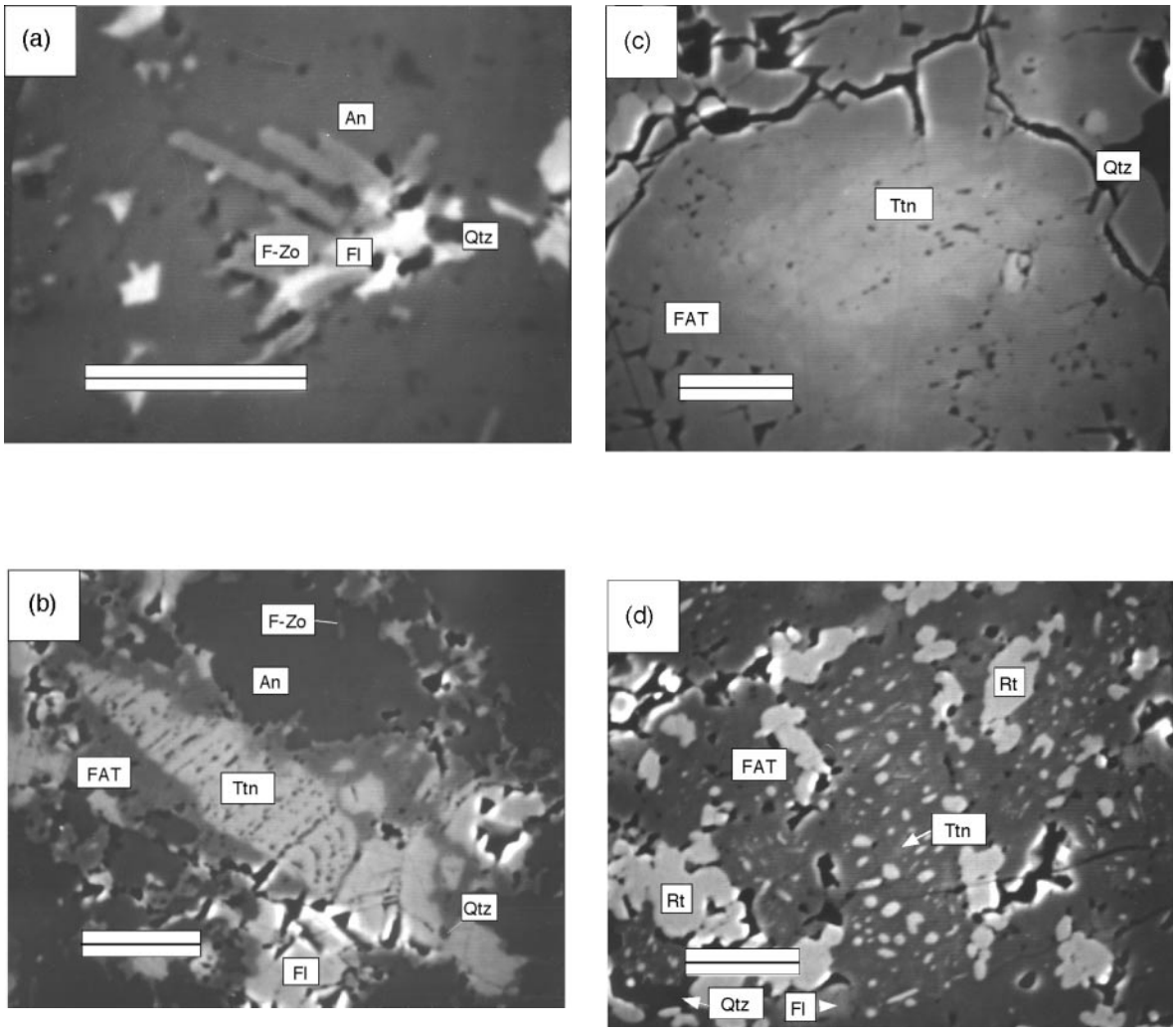

Fig. 3(a)–(d).

similar X_{Al} of 0·50 ± 0·04 and 0·49 ± 0·01 whether the run duration was 8 or 66 h (Fig. 2c).

These results show that newly grown titanite compositions are reproducible and that run durations were sufficient. We take these conditions to reflect equilibrium.

Role of buffering assemblages in F–Al-titanite growth

We explored the role of starting assemblages in F–Al-titanite growth by attempting to grow titanite solid solutions at 1000°C and 2·0 GPa from a range of materials and stoichiometries. The bulk compositions were in the subvolume to the right of the fluorite–anorthite–titanite plane in Fig. 1b.

Examples of run products and typical textures are shown in Fig. 3a–d. The bulk compositions are compared in Fig. 4. Starting mixture A (runs 246 and 228) did not yield F–Al-titanite; however, F-bearing zoisite and quartz nucleated and grew (Fig. 3a). The F–Al-titanite solid solutions grew in all other starting mixtures. The microprobe analyses of titanites were usually performed in the rims of the newly grown titanites. If compositional zoning was visible, the newly grown core was also analysed. In experiments of shorter duration, there is a sharp transition within titanite grains between newly grown F–Al-titanite rims and titanite seeds in the core (Fig. 3b), whereas longer experiments produced a gradual variation in composition from core to rim (Fig. 3c). All run product assemblages included fluorite. Anorthite was partially consumed in all experiments in which F–Al-titanite solid solutions grew (series B–H); in some instances (e.g. run 231) only minor anorthite remained. Most of the experiments had yields of newly grown titanite solid solution. Starting

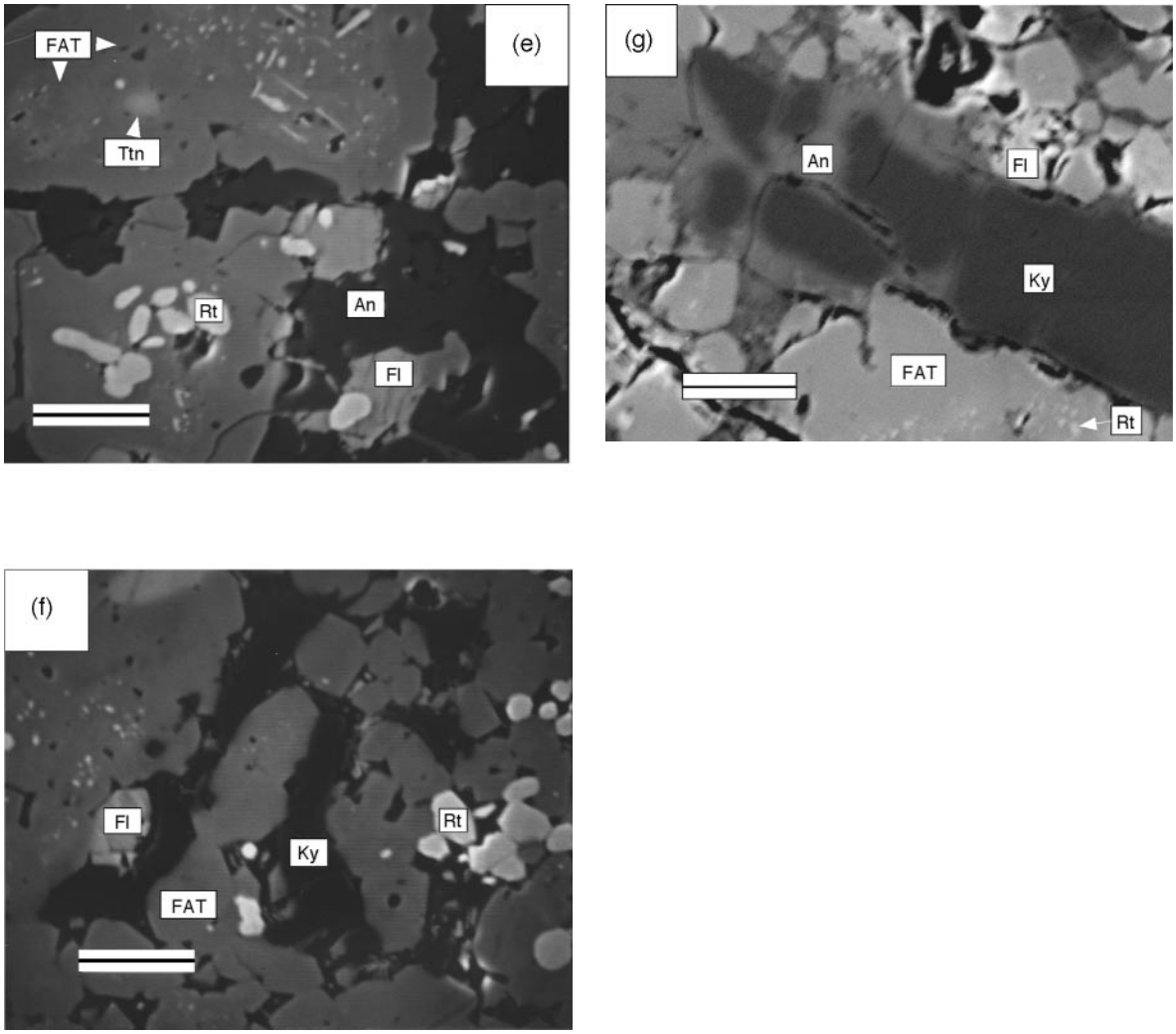

Fig. 3. Back-scattered electron images of experimental run products from experiments at 1000°C and 2 GPa. (a) Blades of F-bearing zoisite (F-Zo) grew in the starting mixture A [anorthite (An) + fluorite (Fl)] in the run product of experiment 246. It should be noted that quartz (Qtz) is also present. The run duration was 46 h. (b) Al–F-titanite (FAT) rims a titanite seed (Ttn) from the starting mixture B [anorthite (An) + fluorite (Fl) + titanite (Ttn) seeds] in the run product of experiment 247; F-bearing zoisite and quartz grow nearby. The run duration was 46 h. (c) Large amounts of newly grown titanite$_{ss}$ (FAT) growing around titanite from the starting assemblage (Ttn) in starting mixture C1 (run 231). Because of the longer run times of 79 h, a diffusive exchange occurs between Ttn and FAT, leading to diffusive grain boundaries. (d) Inclusions of newly formed rutile (Rt) and quartz (Qtz) in Al–F-titanite (FAT) core from run 226. Relicts of the starting titanite (Ttn) remain. The run duration was 114 h. Back-scattered electron images from experimental products of the TARK assemblage (mixture H). (e) Run 242 at 1000°C and 1·2 GPa. The stable assemblage is Al–F-titanite (FAT) + anorthite (An) + rutile (Rt). The growth of rutile needles in the Al–F-titanites should be noted; this indicates that reaction (4) also proceeded simultaneously. (f) Run 236 at 1100°C and 2·0 GPa. The stable assemblage is Al–F-titanite (FAT) + kyanite (Ky) + rutile (Rt); fluorite (Fl) is present in all experimental product assemblages. (g) Run 266 at 1100°C and 1·55 GPa. Anorthite rims kyanite indicating overstepping of reaction (5). The scale bar represents 10 μm in all images.

$CaTiSiO_4O$ was nearly completely consumed (Fig. 3d). Minor corundum grew in experiment run 226. Tiny crystals of newly grown rutile often occur as oriented inclusions in the cores of newly grown F–Al-rich titanite, mostly together with small quartz inclusions (Fig. 3d). In the experiments on the TAFT reaction (4) with mix F, newly grown titanite$_{ss}$ overgrew kyanite. In the experiments at 1·1 GPa and 1·3 GPa at 1000°C and 1100°C, kyanite is rimmed by anorthite, indicating overstepping of the TARK equilibrium (5). Quartz is present in the run products of all experiments.

The experiment with starting mixture B (run 247) yielded <5 μm wide rims of F–Al-titanite that overgrew starting titanite seeds (Fig. 3b). The experimental series with starting mixtures C and D yielded similar results. Mix C1 (run 231) gave high yields of F–Al-titanite, with

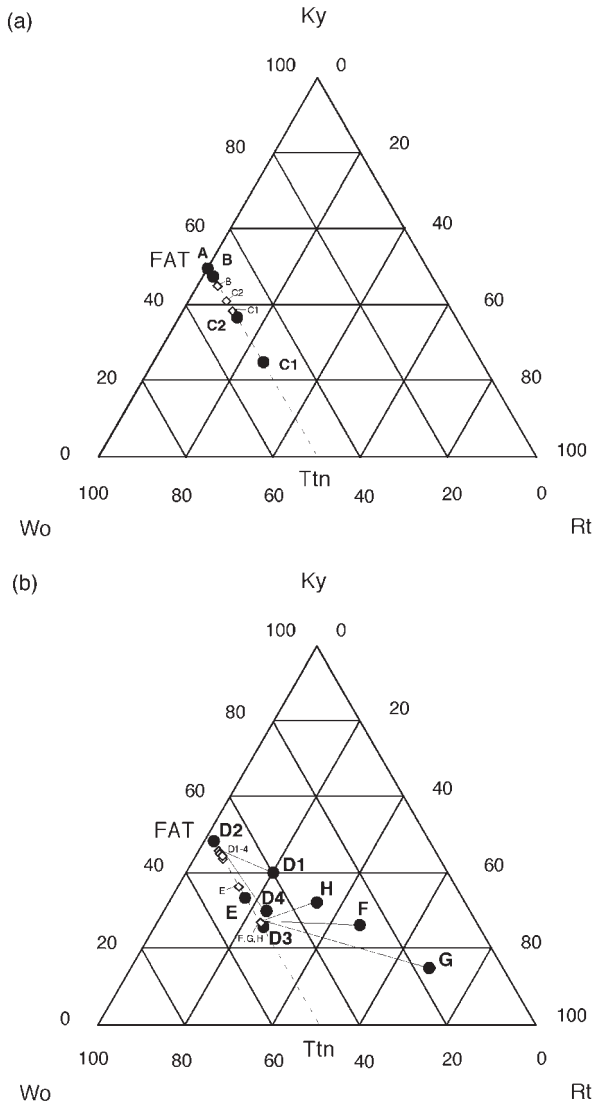

Fig. 4. Compositions of the starting mixtures and the newly grown titanite$_{ss}$ in the wollastonite–kyanite–rutile triangle. (a) Compositions in the system anorthite + fluorite + titanite; ●, mixtures A, B, C1 and C2. ◇, the corresponding F–Al-titanite compositions. (b) Compositions in the system anorthite + fluorite + titanite + kyanite ± quartz; ●, mixtures D1–D4, E, F, G and H; ◇, the corresponding F–Al-titanite compositions. The dashed line indicates the solid solution between titanite $CaTiSiO_4O$ and F–Al-titanite (FAT) $CaAlSiO_4F$.

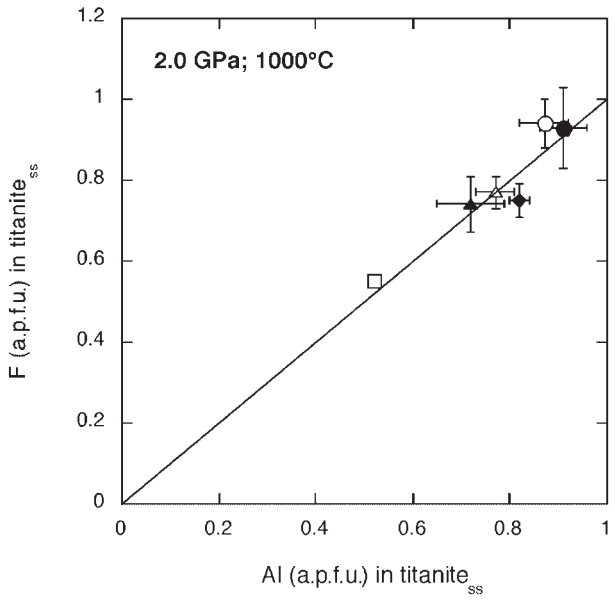

Fig. 5. Compositions of Al–F-titanites from several synthesis experiments at 2·0 GPa and 1000°C. Because of slight F excess (F >1 in several analyses), the diagram has been expanded from 1·0 to 1·2 a.p.f.u. F; ●, starting mix B (anorthite + fluorite + titanite seeds); ○, mix D1 (anorthite + fluorite + kyanite + titanite); △, mix C1 (anorthite + fluorite + anorthite); ◆, mix C2 (anorthite + fluorite + anorthite); ▲, mix E (anorthite + fluorite + quartz + titanite); □, mix F (rutile + fluorite + kyanite + titanite). The standard deviations are 1σ, and are omitted if smaller than the symbol.

crystals larger than 10 μm in diameter and almost no anorthite left (Fig. 3c). The F–Al-rich titanites from this experiment occasionally show zoning with Ti-rich cores and Ti-poor rims. Relict titanite from the starting mixture and quartz crystals also occur in the run products. This kind of zoning was also observed in other experiments, where the Ti-rich cores contain rutile inclusions. Mixtures D1–D4 (runs 233, 79, 80 and 81) and E (run 232) yield substantial volumes of F–Al-rich titanite. Rutile-bearing starting mixtures (F, G and H) yielded newly grown F–Al-titanite and rutile, whereas only small patches of end-member titanite from the starting assemblage remain (Fig. 3d).

The bulk compositions of the starting assemblages of series A–H are linked by tie lines in Fig. 4 to the compositions of titanite that grew in them; titanite compositions are shown alone in Fig. 5 in terms of the extent of F–Al exchange (see Table 1 for average X_{Al} in titanite, and Table 2a–c for representative titanite analyses). For mixture H, we used the titanite composition of experiment 230 at 1000°C and 2·0 GPa. The X_{Al} of titanite$_{ss}$ varies in the experiments from 0·51 ± 0·02 (mixes F, G and H) to 0·91 ± 0·05 (mix B), indicating a wide and continuous range of F–Al-titanite substitution. The errors are 1σ in the mean. The pure F–Al end-member $CaAlSiO_4F$ was never synthesized in the experiments: the titanites always contain some Ti, required by the presence of Ti in all starting mixtures. The F/Al ratio analyzed in titanites from all experiments is 1·01 ± 0·06, indicating a coupled substitution of F with Al. Linking these data to the bulk composition of the buffering assemblages of the mixtures may be depicted in a kyanite–wollastonite–rutile

Table 2c: Electron microprobe analyses of F–Al-titanite from the experiments with bulk composition (series) H

Run no.:	262	251	238	239	269	234	235	237
P (GPa):	1·1	1·2	1·2	1·3	1·35	1·4	1·6	1·8
T (°C):	900	900	1000	1000	1000	1000	1000	1000
n:	5	6	9	14	8	8	10	13
SiO_2	31·97(32)	31·46(49)	31·66(65)	31·42(44)	31·88(31)	31·88(22)	31·60(23)	31·87(56)
TiO_2	25·07(130)	21·39(233)	26·17(222)	21·39(146)	21·24(147)	20·08(81)	21·34(87)	19·65(165)
Al_2O_3	11·48(78)	14·40(108)	11·55(121)	13·70(90)	14·30(88)	14·29(64)	13·43(44)	14·66(114)
CaO	29·46(37)	28·85(66)	26·17(222)	29·68(35)	30·13(61)	29·89(15)	29·74(19)	30·10(64)
F	4·44(32)	5·32(38)	4·69(48)	5·40(43)	5·28(26)	5·62(27)	5·20(20)	5·52(43)
O=F	1·87(14)	2·24(16)	1·97(20)	2·27(18)	2·22(11)	2·37(11)	2·19(09)	2·32(18)
Σ	100·55(46)	100·26(58)	100·13(102)	99·31(53)	100·61(73)	99·39(30)	99·12(23)	99·47(44)
F	0·44(03)	0·53(03)	0·47(05)	0·54(04)	0·52(03)	0·56(03)	0·52(02)	0·54(04)
Si	1·00	1·00	1·00	1·00	1·00	1·00	1·00	1·00
Al	0·42(03)	0·54(04)	0·43(05)	0·51(03)	0·53(03)	0·53(02)	0·50(01)	0·54(04)
Ca	0·99(02)	0·98(01)	0·95(04)	1·01(02)	1·01(02)	1·00(01)	1·01(01)	1·01(03)
Ti	0·59(04)	0·51(06)	0·62(05)	0·51(04)	0·54(04)	0·47(02)	0·51(02)	0·46(05)
Σ	3·00(04)	3·03(03)	3·00(06)	3·04(03)	3·04(02)	3·01(01)	3·02(01)	3·02(04)
X(Al)	0·42(03)	0·51(04)	0·41(05)	0·50(03)	0·51(03)	0·53(02)	0·50(02)	0·54(04)

Run no.:	230	242	243	266	240	245	236
P (GPa):	2·0	1·4	1·5	1·55	1·6	1·8	2·0
T (°C):	1000	1100	1100	1100	1100	1100	1100
n:	4	7	14	12	7	10	8
SiO_2	31·84(31)	31·60(34)	31·46(39)	32·04(23)	31·85(16)	31·81(33)	31·61(53)
TiO_2	20·32(70)	22·44(94)	22·11(143)	21·95(50)	20·72(86)	18·64(179)	20·17(219)
Al_2O_3	13·75(47)	12·80(73)	13·27(95)	13·61(25)	13·70(68)	15·58(122)	14·28(122)
CaO	29·92(16)	29·64(24)	29·68(41)	30·32(27)	29·79(14)	30·24(39)	29·87(45)
F	5·60(20)	4·79(24)	4·91(52)	5·12(14)	5·37(27)	5·77(37)	5·33(49)
O=F	2·36(08)	2·02(07)	2·07(22)	2·15(06)	2·26(11)	2·43(16)	2·24(21)
Σ	99·06(34)	99·25(43)	99·36(44)	100·87(38)	99·17(22)	99·31(32)	99·02(31)
F	0·56(02)	0·48(02)	0·49(05)	0·50(01)	0·53(02)	0·57(03)	0·53(04)
Si	1·00	1·00	1·00	1·00	1·00	1·00	1·00
Al	0·51(01)	0·48(02)	0·50(03)	0·50(01)	0·51(02)	0·58(04)	0·53(04)
Ca	1·01(01)	1·01(02)	1·01(01)	1·01(01)	1·00(00)	1·02(01)	1·01(01)
Ti	0·48(02)	0·53(03)	0·53(04)	0·52(01)	0·49(02)	0·44(05)	0·48(06)
Σ	3·00(02)	3·02(03)	3·04(02)	3·03(01)	3·00(01)	3·04(02)	3·03(04)
X(Al)	0·51(02)	0·47(02)	0·48(03)	0·49(01)	0·51(02)	0·57(04)	0·53(05)

All formulae are normalized to 1 Si; *X*(Al), [Al/(Al + Ti)]; numbers in parentheses are 1σ standard deviations; *n*, number of analyses.

triangle (Fig. 4). These data indicate that the starting composition is not relevant and the final titanite composition depends on *P*, *T* and the final buffering assemblage.

The *P–T* dependence of the F–Al substitution in titanite

Another set of experiments explored the dependence of F–Al substitution in titanite on *P* and *T*. This requires

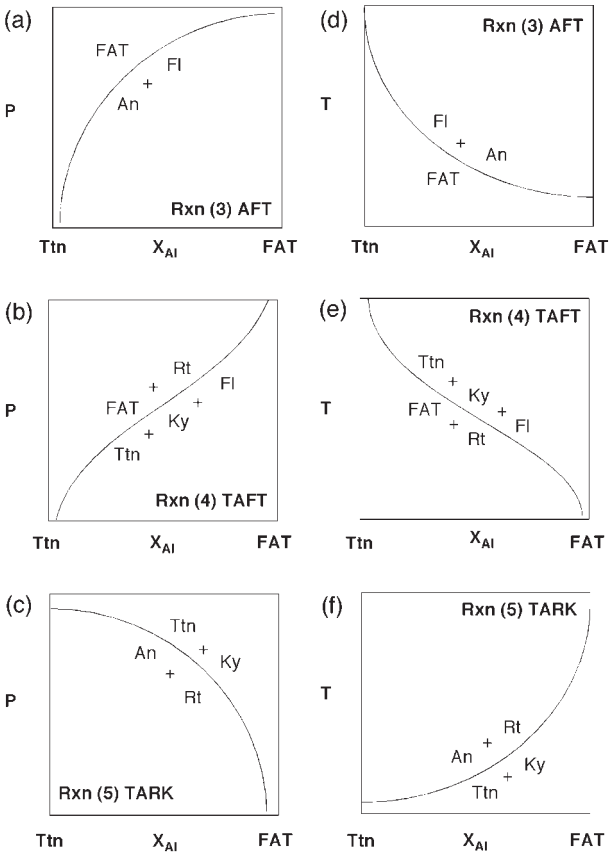

Fig. 6. Schematic P–X_{Al} and T–X_{Al} diagrams to illustrate the compositional changes of titanite solid solution along reactions (3)–(5).

an appropriate mineral assemblage to simultaneously buffer the compositions of the F–Al and Ti–O components of titanite solid solutions. If the titanite composition is a binary solid solution, as required by the Gibbs–Duhem equation, this condition is met by reactions (3)–(5). In this study, we explored the P–T dependence with the TAFT reaction (4). Starting mixtures F and H, which contained kyanite, rutile, fluorite, titanite ± anorthite (Table 1), were utilized in these experiments. At high P and T, reaction (4) is driven to the right as F–Al-titanite and rutile grow at the expense of kyanite, titanite and fluorite, until equilibrium titanite compositions are generated. Representative compositions are given in Table 2b. In contrast to the reactions involving anorthite + fluorite, these experiments never yielded F-bearing zoisite.

Pressure dependence

Figure 6a–c shows schematically the predicted shapes of reactions (3)–(5) in a P–X_{Al} diagram. Reaction (3), AFT, will increase in pressure with increasing Al substitution in titanite, whereas reaction (5), TARK, will decrease in pressure with increasing Al substitution in titanite. Reaction (4), TAFT, also has a positive slope, which changes for intermediate values of X_{Al}. The pressure dependence of titanite composition in the TAFT equilibrium was investigated at a range of pressures at 900°C, 1000°C and 1100°C (Table 1). New F–Al-titanite and rutile grew in all runs, as demonstrated by F–Al-titanite rims on titanite, and rutile inclusions with or without quartz or coesite in F–Al-titanite (Fig. 3d). Rutile clearly grew during these experiments, as its modal abundance strongly increases. In contrast to rutile from the starting material, the newly grown rutiles are extremely small and form oriented inclusions in cores of newly formed F–Al-titanites. In two experiments (46 and 256) with mixture F at 1·1 GPa at 1000°C and 1·3 GPa at 1100°C, anorthite grew in addition to F–Al-titanite and rutile. This is similar to experiments with mixture H below 1·2 GPa at 900°C, 1·4 GPa at 1000°C and 1·6 GPa at 1100°C (262, 238, 239, 249, 242, 243 and 248), where kyanite was nearly completely consumed and is rimmed by anorthite.

The change in X_{Al} of newly grown titanite$_{ss}$ with pressure is given in Table 2b and displayed in Fig. 7a and b, illustrating the results from mixtures F (Fig. 7a and b) and H (Fig. 7b). Values of the X_{Al} in mixture F increase with increasing pressure at 900°C, 1000°C and 1100°C, with values ranging from 0·33 ± 0·05 to 0·57 ± 0·01 (Fig. 7a, Table 2). The change in composition with pressure is greater when titanite coexists with anorthite below the TARK equilibrium than with kyanite above it (Fig. 7a). At any given pressure, titanite composition buffered by the TAFT equilibrium is the same at 1000 and 1100°C. The results with mixture H are similar (Fig. 7b). Values of X_{Al} increase with increasing pressure at 900°C from 0·42 to 0·48, at 1000°C from 0·41 to 0·54, and at 1100°C from 0·47 to 0·54 (Fig. 7b, Table 2c).

Temperature dependence

The starting assemblage kyanite + rutile + fluorite ± anorthite + titanite (series F and H) was also run at temperatures of 900°C, 1000°C and 1100°C. Mixture F was run at 2·0 GPa to investigate the temperature dependence of the F–Al substitution in titanite (Table 2b). Along with the starting assemblage, only newly grown F–Al-titanite and quartz were present in the run products; no anorthite was observed. Figure 6d–f shows schematically the predicted shapes of reactions (3)–(5) in a T–X_{Al} diagram. Reaction (3), AFT, will decrease in temperature with increasing Al substitution in titanite, whereas reaction (5), TARK, will increase in temperature with increasing Al substitution in titanite. Reaction (4), TAFT, also has a positive slope, which changes for intermediate values of X_{Al}. Figure 7c shows that at 2·0 GPa X_{Al} decreases from 0·55 ± 0·03 to 0·51 ± 0·01 as temperature rises

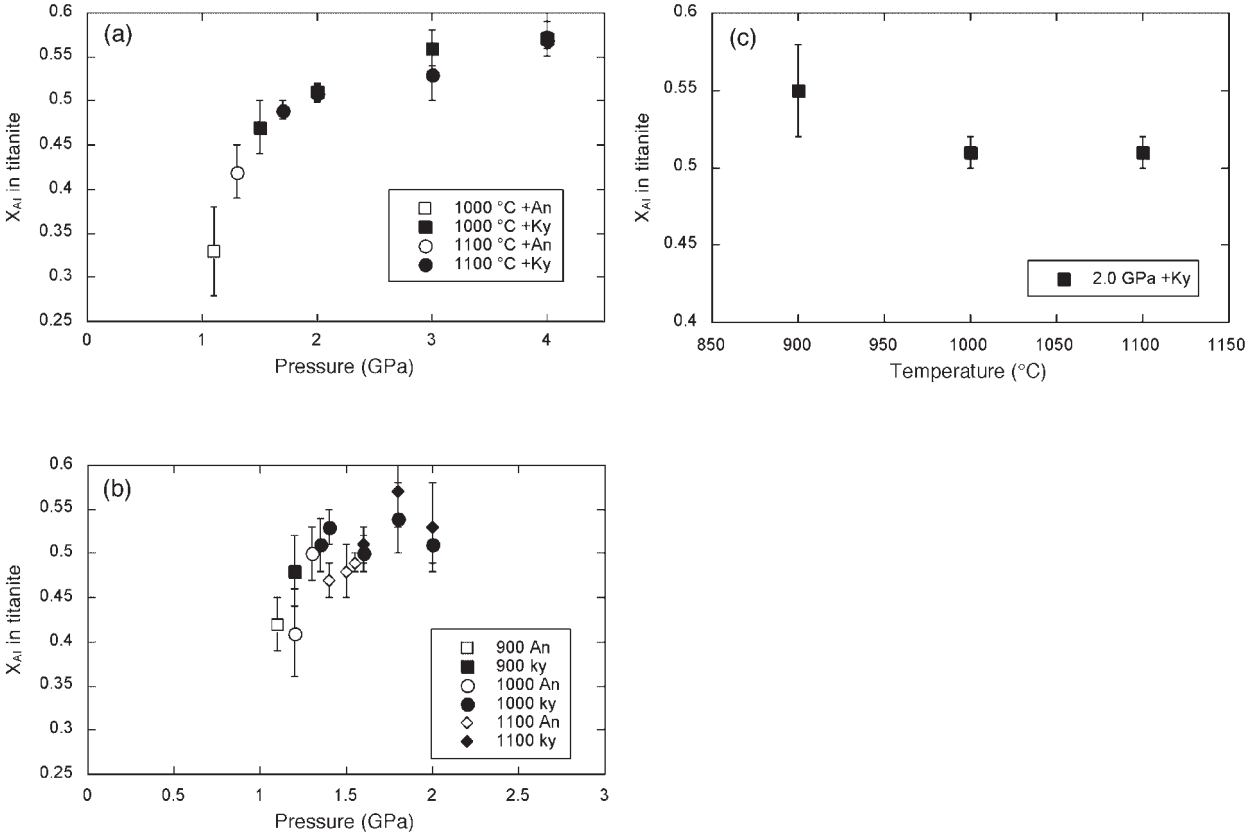

Fig. 7. Plot of X_{Al} in titanite$_{ss}$ vs P (a), (b) and T (c). (a) Results from the experiments with series F; □, experiments at 1000°C with anorthite; ■, experiments at 1000°C with kyanite; ○, experiments at 1100°C with anorthite; ●, experiments at 1100°C with kyanite. (b) Results from the experiments with mixture H. Open symbols show experiments with anorthite as part of the stable assemblage, filled symbols show experiments with kyanite as part of the stable assemblage. (c) ■, experiments at 2·0 GPa with kyanite. The standard deviations are 1σ.

from 900°C to 1000°C. At 1100°C, X_{Al} is the same as at 1000°C.

Mixture H was run at 1·4, 1·6, 1·8 and 2·0 GPa at 1000°C and 1100°C. In the experiments at 1·6–2·0 GPa, no change in X_{Al} was found (Fig. 7b). Only in the experiments at 1·4 GPa did X_{Al} increase with falling temperatures, from 0·48 to 0·53; this effect is probably due to the change in the assemblage from anorthite at 1100°C to kyanite at 1000°C.

Displacement of the TARK equilibrium through addition of CaF_2

The addition of fluorite to the assemblage anorthite + rutile + titanite + kyanite shifts the TARK equilibrium to lower pressures from the experimentally determined reversals (Manning & Bohlen, 1991). In the experiments at 900°C, only minor reaction occurred at 1·2 GPa. In contrast, the reaction direction could easily be determined in the experiment at 1·1 GPa where anorthite overgrew kyanite. Small (<3 μm) dendritic crystals of a Ca–Al-rich phase grew in one run (run 245), possibly indicating a small degree of melting. In many experiments where Al–F-titanite overgrew starting titanite, no sharp grain boundary existed between the two minerals (Fig. 3e and f). Figure 3e shows that some Al–F-titanites display a slight zoning with brighter Ti-enriched cores, containing numerous inclusions of rutile, and darker Ti-poor rims. In the experiments at 1·1 and 1·2 GPa (runs 251 and 262) at 900°C, 1·30, 1·35 and 1·40 GPa (runs 239, 249, 269, and 234) at 1000°C, and 1·55 and 1·60 GPa (runs 248, 266 and 240) at 1100°C, the isobaric or isothermal invariant assemblage Al–F-titanite + anorthite + kyanite + rutile + fluorite remained. In the experiments at 900°C and 1·1 GPa (run 262), 1000°C and 1·30 GPa (run 239), and 1100°C and 1·55 GPa (runs 248 and 266), anorthite overgrows kyanite, indicating the overstepping of the TARK reaction (5), as shown in Fig. 3g. In the experiments above 1·35 GPa at 1000°C and 1·55 GPa at 1100°C, the modal amount of anorthite strongly decreases with the formation of Al–F-titanite and kyanite (Fig. 3f). Below 1·3 GPa at 1000°C and 1·5 GPa at 1100°C, kyanite disappeared (Fig. 3e). Rutile is stable throughout the range of investigation, and tiny, newly

Table 3: Electron microprobe analyses of anorthite and kyanite

Run no. (series):	248 (H)	234 (H)	240 (H)
P (GPa):	1·55	1·4	1·6
T (°C):	1100	1000	1100
n:	2	3	3
SiO_2	43·08(03)	37·22(04)	37·58(43)
TiO_2	0·21(15)	0·31(08)	0·32(12)
Al_2O_3	35·81(41)	62·93(11)	37·58(43)
CaO	20·55(22)	0·63(03)	0·55(12)
F	0·41(20)	0·07(02)	0·29(12)
O=F	0·17(08)	0·03(01)	0·12(05)
Σ	99·89(05)	101·12(15)	100·60(56)
F	0·06(03)	0·01(00)	0·01(01)
Si	2·00	1·00	1·00
Al	1·96(02)	1·99(01)	1·94(03)
Ca	1·02(01)	0·02(00)	0·02(00)
Ti	0·01(01)	0·01(00)	0·01(00)
Σ	4·99(00)	3·02(01)	2·97(02)

Anorthite formulae normalized to 2 Si, kyanite formulae normalized to 1 Si; numbers in parentheses are 1σ standard deviations; *n*, number of analyses.

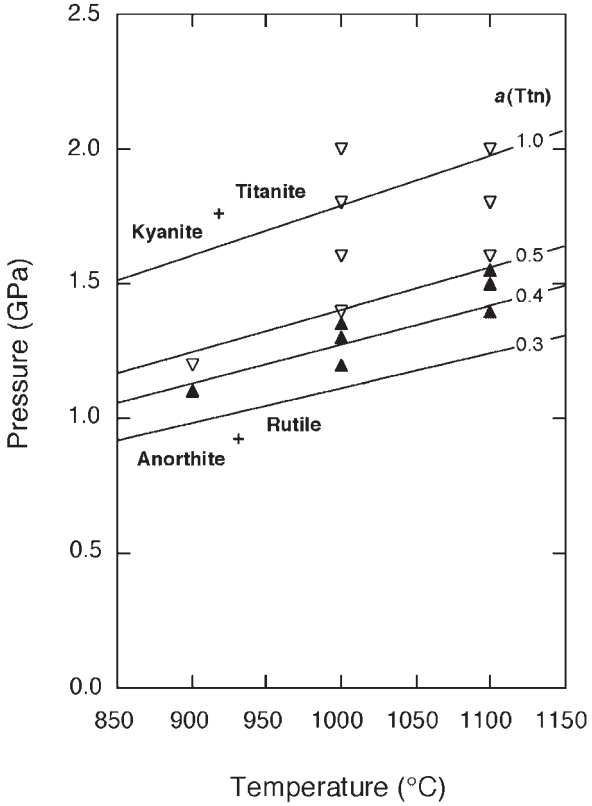

Fig. 8. The end-member curve of reaction (5) calculated with different titanite activities with the program THERMOCALC v. 2.7 and the database of Holland & Powell (1998). The numbers on the curves indicate the activity of titanite. ▽, growth of (Al + F) titanite + kyanite + rutile; ▲, (Al + F) titanite + anorthite + rutile growth.

formed rutile needles are always found as inclusions in Al–F-titanite. Two experiments with mixture H (runs 243 and 266) also showed small amounts of corundum. Although all experiments contain small amounts of quartz, it occurs only as inclusions in F–Al-titanite, and thus is never found in contact with corundum.

The chemical data from the experiments with assemblage H are shown in Table 2c. The (Al + F) content in titanite does not exceed 0·63. The total variation in X_{Al} is between 0·38 and 0·54 at 900°C, 0·37 and 0·59 at 1000°C, and between 0·42 and 0·63 at 1100°C. Overall, the data show a slight decrease in X_{Al} when titanite$_{ss}$ coexists with the assemblage anorthite + rutile + fluorite. Some titanites contain slightly more titanian cores (X_{Al} of 0·4). Kyanite and anorthite were also analyzed (Table 3). Kyanite contains small amounts of F (0·003–0·033 a.p.f.u.) and Ca (0·011–0·019 a.p.f.u.), and its mole fraction of Al [Al/(Al + Ti)] is therefore very close to unity (0·995–0·998). Anorthite shows a slight Al deficiency (1·96 ± 0·02 a.p.f.u.) and also contains small amounts of F (0·06 ± 0·03 a.p.f.u.) and Ti (0·01 ± 0·01 a.p.f.u.). Owing to the small grain size of the newly formed rutile needles, no reliable analyses could be obtained, although previous experimental studies suggest minor Al (0·02 a.p.f.u.) in rutile (Manning & Bohlen, 1991).

Above 1·35 GPa at 1000°C and 1·6 GPa at 1100°C, anorthite rapidly disappears, as does kyanite below these pressures. Because our experiments were conducted at 900°C, 1000°C and 1000°C, the calculated positions of the TARK equilibrium from Holland & Powell (1998) at 1·60 GPa at 900°C, 1·79 GPa at 1000°C and 1·98 GPa at 1100°C were used to determine the extent of the shift. The locus of this curve shifted to 1·1–1·2 GPa at 900°C, 1·30–1·35 GPa at 1000°C and 1·55–1·6 GPa at 1100°C (Fig. 8). Taking the midpoints of the brackets, the displacement in pressure is 0·45 GPa at 900°C, 0·46 GPa at 1000°C and 0·405 GPa at 1100°C. Figure 8 shows equilibrium (5) with activities of $CaTiSiO_4O$ in titanite ranging from 1·0 to 0·3, assuming the other phases are stoichiometric, along with the experimental results of this study. The curves were calculated with the updated version of the program THERMOCALC v. 2.7 (T. J. B. Holland, personal communication, 1999) and the database of Holland & Powell (1998). The experiments show that the magnitude of displacement decreases with rising temperature, which requires that the activity of $CaAlSiO_4F$ in titanite solid solution buffered

by anorthite + kyanite + rutile + fluorite increases with rising temperature.

DISCUSSION

Our results show that: (1) equilibrium compositions were obtained; (2) it is possible to synthesize highly aluminous (X_{Al} >0·5) F–Al-titanites at 1000°C and 2·0 GPa; (3) a continuous solid solution exists in titanites in the compositional range of our investigation (X_{Al} = 0·33–0·91); (4) titanite seeds in the starting material are needed for the nucleation of F–Al-titanite (Troitzsch & Ellis, 1999). In addition, compositions of the newly grown titanite solid solutions show equality of F and Al concentrations in F–Al-titanite, which indicates that OH substitution for F (vuagnatite-type substitution), if it is present, is too minor to detect. Product assemblages included titanite$_{ss}$ + anorthite + fluorite, titanite$_{ss}$ + anorthite + kyanite + fluorite, titanite$_{ss}$ + anorthite + quartz + fluorite and titanite$_{ss}$ + kyanite + rutile + fluorite. The relationship between the growth of titanite solid solutions and variable compositions in different starting assemblages will be discussed below. In the presence of the assemblage titanite$_{ss}$ + kyanite + rutile + fluorite, X_{Al} in titanite is fixed at constant P and T and varies only slightly with changes in P and T.

Constraints on P–X_{Al} and T–X_{Al} phase relations

The phase relations implied by our experiments may be interpreted in terms of isothermal P–X_{Al} and isobaric T–X_{Al} diagrams (Fig. 9a–d). In these diagrams, the positions of reactions (3), (4) and (5) are calculated with the activities obtained above and the compressibility and expansivity data from Table 4. These reactions intersect in an isothermal or isobaric invariant point. The titanite compositions in the presence of rutile, kyanite and fluorite define the position of TAFT. Experiments in which anorthite coexists with fluorite, titanite and either rutile or kyanite constrain the position of AFT. The TARK equilibrium shifts with X_{Al} from the end-member position to the isobaric–isothermal invariant point (Fig. 9).

The position of TAFT is constrained by kyanite-bearing, anorthite-free product assemblages. The TAFT reaction shifts to intermediate compositions because of the capability of mutual solution of titanite and Al–F-titanite phase components. Above 1·2 GPa at 900°C, Al–F-titanite coexists with kyanite and X_{Al} increases to 0·51–0·55 (Fig. 9a). This increase in X_{Al} was also observed in the experiment series with mixtures F and H at 1000°C and 1100°C where X_{Al} ranges from 0·33 to 0·48 in the presence of anorthite and 0·50 to 0·54 in the presence of kyanite (Fig. 9b and c). Thus, there is little change in X_{Al} with pressure in equilibrium with rutile, kyanite and fluorite at the conditions investigated. TAFT therefore has a steep slope in P–X_{Al} and T–X_{Al} space (Fig. 9).

The location of TAFT shown in Fig. 9 is consistent with results of Smith (1981). At 1100°C and 2·0 GPa, Smith (1981) generated a Ca–Al silicate melt coexisting with rutile, fluorite and corundum. In addition, he reported that 'several' run products also contained 'fluorite or quartz or kyanite' in experiments at 1100–1200°C and 1·5–3·5 GPa. We interpret this to mean that fluorite, quartz and kyanite did not all coexist with rutile and titanite in any of his experiments. The absence of full TAFT assemblage, combined with the presence of melt and corundum in his experiments, probably results, at least in part, from the fluorite-poor, rutile–kyanite-rich bulk compositions he used. Regardless, the lower Al content of titanite reported by Smith (1981) is consistent with the phase relations depicted in Fig. 9b, in that titanite coexisting with rutile, in the absence of kyanite and fluorite, should be less aluminous than titanite buffered by the TAFT assemblage.

Anorthite-bearing, kyanite-free product assemblages constrain the P–X_{Al} and T–X_{Al} geometry and provide an upper pressure bound for the AFT reaction (Fig. 9c). In addition, our unreversed experiments on bulk compositions C–E also provide a maximum P limit on AFT at high X_{Al} (Fig. 9b).

Figure 9a–d shows that the isothermal–isobaric invariant point of reactions (3)–(5) intersects at intermediate X_{Al} of 0·5. The change in assemblage explains the large shift in titanite composition, owing to the shallower slope of this reaction. In addition, the different assemblages and F–Al-titanite compositions at 1·1–1·2 GPa and X_{Al} ~0·40–0·50 at 900°C, 1·30–1·35 GPa and X_{Al} ~0·45–0·50 at 1000°C, and 1·55–1·60 GPa and X_{Al} ~0·50 at 1100°C set a firm constraint on the position of the invariant point (Fig. 9a–d).

Figure 9d shows the inferred phase relations at 2·0 GPa as a function of temperature and X_{Al}. Our experiments at 900–1100°C imply that the titanite compositions in the TAFT assemblage shift to increasing X_{Al} with falling temperature at constant pressure. The small change in the pressure of the invariant point between 900 and 1100°C leads us to suggest that it lies at >1300°C at 2·0 GPa, although it seems reasonable to expect that it will occur at similar X_{Al} as at 900°C, 1000°C and 1100°C. As discussed above, the low-Al titanites coexisting with rutile of Smith (1981) are consistent with the absence of fluorite + kyanite + quartz in his run products.

The compositions of titanite solid solutions associated with different mineral assemblages can be inferred from Fig. 9a–d and can be summarized on P–X_{Al} and T–X_{Al} diagrams by considering coexistence of quartz/coesite with fluorite, aluminosilicate, or rutile (Fig. 10a–c). In the presence of quartz/coesite and fluorite (Fig. 10a),

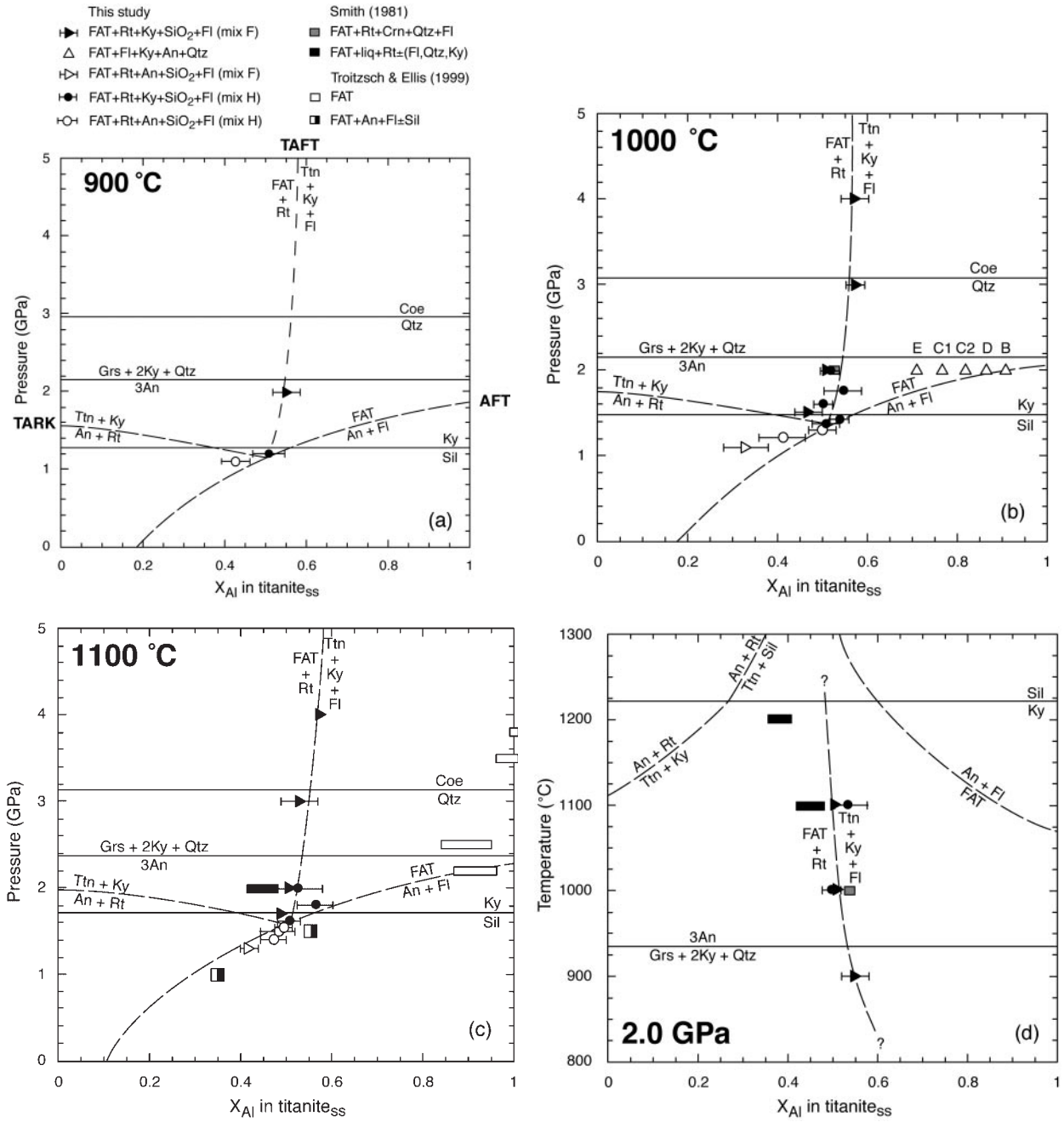

Fig. 9. P–X_{Al} diagrams illustrating the Al–F content in titanite solid solution as a function of pressure. The experiments were conducted with the assemblage kyanite + rutile + fluorite + titanite and are compared with the experiments of Smith (1981) (■ and grey squares) and the experiments of Troitzsch & Ellis (1999) (□ and half-black squares). ▶, assemblage Al–F-titanite + kyanite + rutile + fluorite; ▷, assemblage Al–F-titanite + anorthite + fluorite ± rutile ± quartz. △, results of the experiments with starting mixtures A–E, which help to put a constraint on reaction (3). Also shown are the reactions quartz = coesite, kyanite = sillimanite and 3anorthite = grossular + 2kyanite + quartz. The position of these reactions was calculated with the database of Holland & Powell (1998). The positions of reactions (3) and (5) from the text were calculated with the available volume data from Table 4. The position of reaction (4) was drawn based on the experimental constraints. (a) P–X_{Al} diagram at 900°C; (b) P–X_{Al} diagram at 1000°C; (c) P–X_{Al} diagram at 1100°C; (d) T–X_{Al} diagram illustrating the Al–F content in titanite solid solution as a function of temperature at 2·0 GPa. The standard deviations are 1σ.

Table 4: Volume, compressibility and expansivity data used in thermodynamic calculations

Phase	$V°_{298·15}$	Ref.	a (10^{-5})	b (10^{-9})	Ref.	c (10^{-6})	d (10^{-12})	Ref.
Anorthite	10·079	(1)	1·252	2·209	(1)	−1·084	2·562	(1)
Rutile	1·882	(1)	2·322	4·156	(1)	−0·449	0·426	(1)
Kyanite	4·414	(1)	2·125	3·765	(1)	−0·629	0·948	(1)
Titanite	5·565	(1)	2·216	3·840	(1)	−0·907	1·851	(1)
FAT	5·181	(2)	2·216	3·840	(1)	−0·907	1·851	(1)
Fluorite	2·454	(3)	0·524	0·312	(4)	−1·081	−0·349	(5)

$V°_{298·15}$ in J/bar; $V_{P,T} = V°_{298·15} + [V°_{298·15}\, a(T - 298·15)] + [V°_{298·15}\, b(T - 298·15)] + [V°_{298·15}\, c(P - 1)] + [V°_{298·15}\, d(P - 1)^2]$, P in bar; T in K. For most minerals, the data from Holland & Powell (1998) were refitted to the equation above. Ref. (reference): (1) Holland & Powell (1998); (2) Troitzsch & Ellis (1999); (3) Robie & Hemingway (1995); (4) this study; (5) Vaiyda *et al.* (1973).

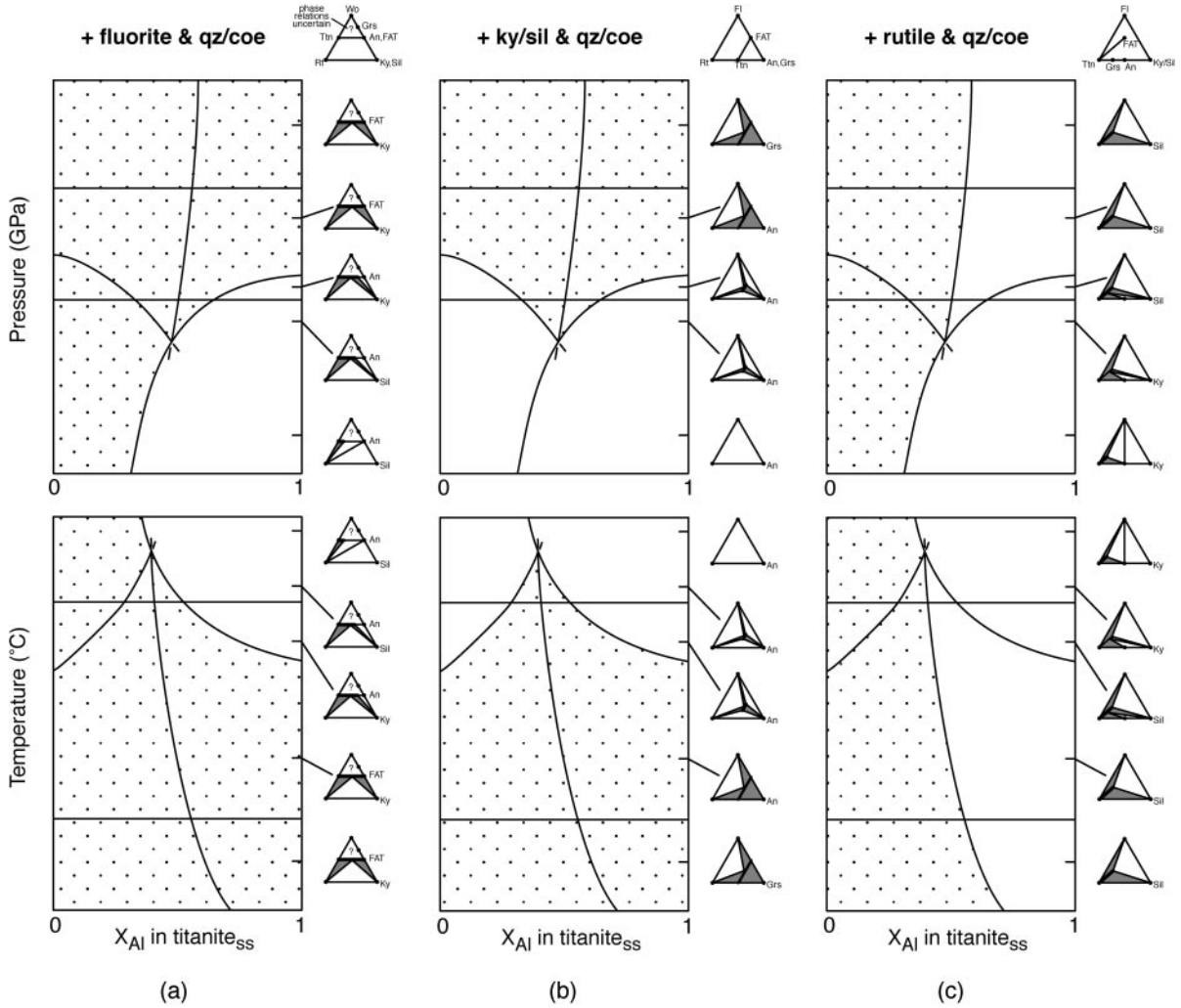

Fig. 10. Schematic P–X_{Al} and T–X_{Al} diagram with compositional ternaries. These diagrams are based on the P–X_{Al} and T–X_{Al} plots from Fig. 9. The labels of the three curves (AFT, TARK and TAFT) are the same as in Fig. 9 and have been omitted for clarity. The diagrams illustrate the range of Al + F substitution in titanite$_{ss}$ coexisting with any of the assemblages fluorite + quartz/coesite, kyanite/sillimanite + quartz/coesite and rutile + quartz/coesite, as indicated by the stippled area.

titanite solid solution is stable only in the stippled regions of the relevant P–X_{Al} and T–X_{Al} diagrams. The AFT equilibrium requires that as pressure decreases or temperature rises, the maximum Al in titanite decreases. In the wollastonite–rutile–kyanite ternary, phase relations are uncertain above the titanite–anorthite/F-titanite join because these Ca-rich bulk compositions are not yet fully investigated (Tropper, 1998). With increasing pressure at constant temperature (or falling temperature at constant pressure) the two-phase field (+ fluorite, + SiO_2) for rutile + titanite of variable composition expands, and the X_{Al} in titanite coexisting with rutile and anorthite increases to a maximum at the intersection, where the discontinuous TARK reaction limits stability of this assemblage to higher presssure (or lower temperature). Beyond the intersection, kyanite + rutile coexist with titanite of increasing X_{Al}, and the two-phase field titanite + rutile continues to expand. The maximum X_{Al} in titanite coexists with anorthite and fluorite and kyanite, until the stoichiometric AFT reaction (1) is crossed. At higher pressures or lower temperatures, anorthite and fluorite are no longer stable together because of end-member F–Al-titanite stability.

In the presence of stable Al_2SiO_5 and SiO_2 polymorphs, $titanite_{ss}$ is limited to pressure above (or temperature below) the intersection (Fig. 10b). With increasing pressure (falling temperature), the first titanite to form is therefore intermediate, and the compositional range permitted with Al_2SiO_5 expands as pressure increases further. At a fixed P and T below the end-member TARK and AFT reactions, there are thus three three-phase fields (+ Al_2SiO_5 and SiO_2) with invariant titanite compositions in the fluorite–rutile–anorthite ternary (anorthite + rutile + titanite, rutile + fluorite + titanite, and anorthite + fluorite + titanite) and three two-phase fields in which titanite composition is variable (titanite + anorthite, titanite + rutile, and titanite + fluorite). At higher pressure (or lower temperature), titanite of variable composition can coexist with anorthite or grossular (+ Al_2SiO_5 + SiO_2) but not fluorite, or fluorite or rutile but not anorthite or grossular. The three-phase assemblage rutile + fluorite + titanite is stable to high pressure, but titanite composition is fixed at constant P and T.

Titanite solid solutions coexisting with rutile are always low in X_{Al}, because they must lie to the left of the TAFT equilibrium (Fig. 10c). In this compositional region, the only important reaction encountered with increasing pressure (falling temperature) is the TARK equilibrium, along which titanite composition is fixed at any P and T. The maximum X_{Al} of titanite solid solution in the presence of rutile and SiO_2 occurs with fluorite and either anorthite or Al_2SiO_5.

Figure 11 shows the relative changes in the phase relations in terms of approximate P, T and titanite composition. The small P and T dependence of phase relations in this system implies that the AFT reaction lies at a similar P and T, and has a similar slope, as the TARK reaction, at least at >800°C. This means that the invariant point shifts little in terms of X_{Al}. The main change in Fig. 11 is that the kyanite–sillimanite equilibrium crosses the invariant point between 1000°C and 1100°C.

Growth of F-zoisite and quartz

Minor quantities of F-bearing zoisite and quartz grew in all anorthite-rich bulk compositions. F-zoisite was not observed in bulk compositions with high TiO_2/CaF_2 ratios (series E–H, Table 1). Zoisite, $Ca_2Al_3Si_3O_{12}(OH)$, has the hypothetical fluorian analogue $Ca_2Al_3Si_3O_{12}F$ which, like F–Al-titanite, is collinear with anorthite and fluorite (Fig. 3b) as can be seen from the reaction

$$3CaAl_2Si_2O_8 + CaF_2 = 2Ca_2Al_3Si_3O_{12}F \quad (8)$$

Anorthite + Fluorite = F-Zoisite.

However, because F-zoisite probably contains both F and OH, it may be stabilized by an additional component, such as H_2O. The presence of H_2O could have an influence on the stability of FAT by leading to a solid solution between FAT and the Al–OH end-member $CaAlSiO_4OH$ (vuagnatite, McNear *et al.* 1976) although preliminary experimental investigations by Fehr (1991) showed that vuagnatite is stable only at low temperatures (<290°C at 0·3 GPa, <600°C at 3·0 GPa). The occurrence of H_2O in the capsule either through moisture in the air or fluid inclusions in the natural fluorite, allows F_2-producing reactions such as

$$3CaAl_2Si_2O_8 + CaF_2 + H_2O = 2Ca_2Al_3Si_3O_{12}(F_{0.5}OH_{0.5}) + 0{\cdot}5F_2 + 0{\cdot}5H_2 \quad (9)$$

Anorthite + Fluorite + H_2O = F–OH-Zoisite + Fluorine + Hydrogen.

Reactions (8) and (9) are written with representative starting minerals as reactants. Many reactions were proceding simultaneously in these experiments, so these reactions are several of the numerous possible pathways for the production of F–OH-zoisite.

Fluorine contents of analyzed zoisites range from 1·11 to 1·78 wt % or 0·27 to 0·42 F per formula unit (Table 5). The low analytical totals and F <1 imply the presence of additional OH or O. Troitzsch & Ellis (1999) also reported F-zoisite. They confirmed the presence of OH by IR spectroscopy and energy-dispersive analysis for oxygen. IR spectroscopy was not possible with the zoisite from our study because of small crystal sizes (<2–3 μm) and low yields, but we assume that the electric charge imbalance in our zoisites is also accommodated by OH.

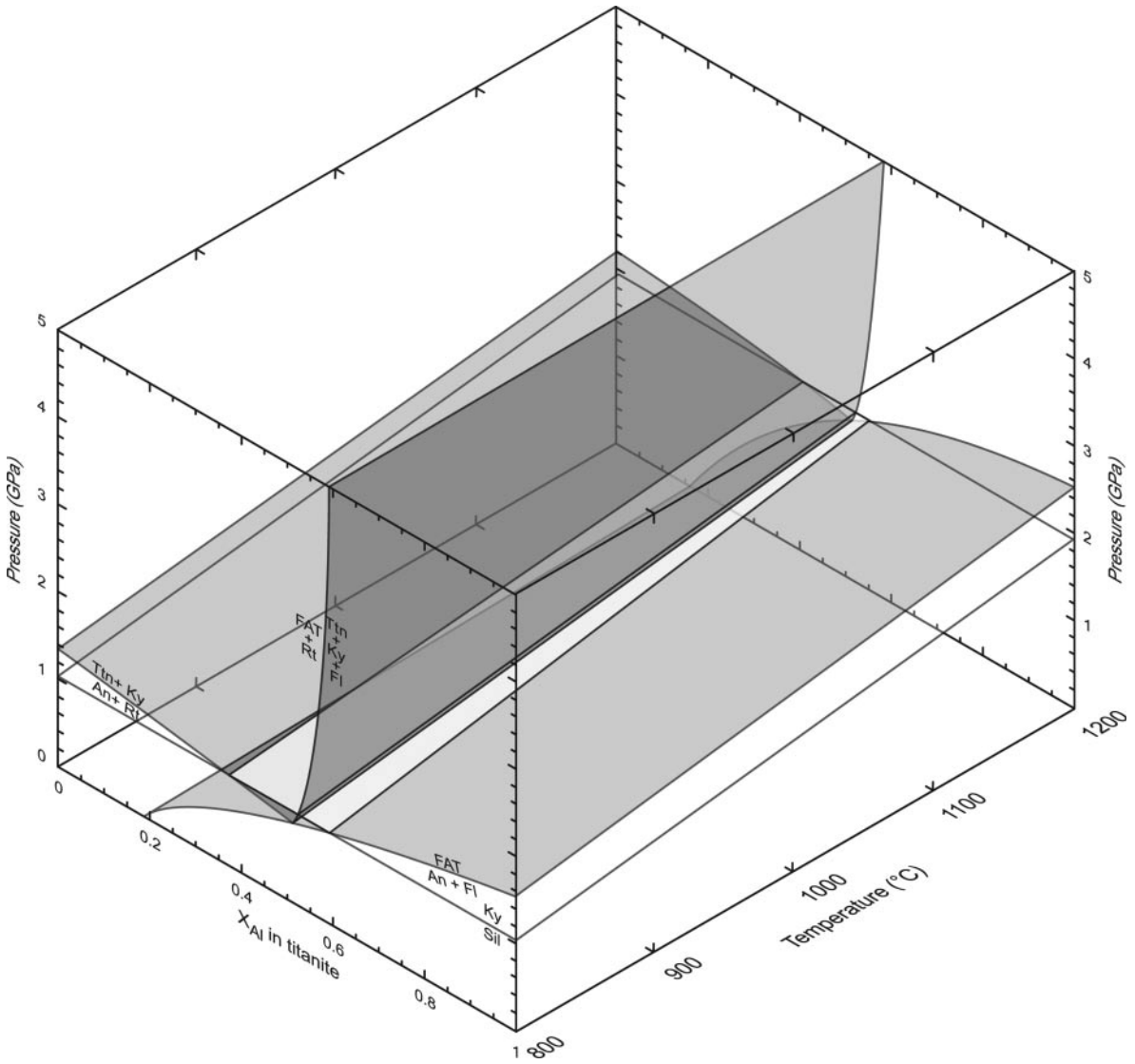

Fig. 11. Schematic P–T–X_{Al} diagram illustrating phase relations involving titanite solid solution at high temperature and pressure.

The growth of minor F- and OH-bearing zoisite implies that small amounts of H_2O were incorporated into the charges although the experiments were nominally H_2O-free.

There are several possible explanations for the growth of hydrous phases during nominally anhydrous experimental conditions: (1) water contamination during welding; (2) presence of water in the natural minerals; (3) incomplete dehydration or dehydroxylation during drying treatment before experiments; (4) exchange of H_2O, H_2 or O_2 across capsule walls during experiments. Although we used the standard method of drying capsules at 110°C before welding, the welding step itself could lead to reintroduction of some water into the charge. This is because welding of the $Ag_{80}Pd_{20}$ capsules in air requires rapid conduction of heat away from the weld, which is done by wrapping the capsule in a water-moistened tissue. Water and/or moist air could thus be trapped in the capsule as it is welded shut. Troitzsch & Ellis (1999) suggested that this was the source of water in F-zoisites in their run products.

In addition to contamination during welding, water could have been been introduced into some of our experiments via fluid inclusions in natural phases, particularly fluorite. Run numbers 18–120 used unfired natural fluorite. However, this cannot be the sole source of H_2O because experiments using synthetic fluorite, fired at 950°C, also produced F-zoisite. Nonetheless, slightly higher modal abundances of F-zoisite were observed in runs with natural fluorite.

Table 5: Electron microprobe analyses of F-bearing zoisite

	1	2	3	4
SiO_2	39·57	39·56	39·74	39·15
TiO_2	0·08	n.d.	n.d.	n.d.
Al_2O_3	32·67	33·87	33·15	33·10
CaO	25·31	24·20	24·38	24·59
F	1·47	1·23	1·78	1·11
O=F	0·62	0·52	0·75	0·47
Σ	98·48	98·34	98·32	97·59
F	0·35	0·30	0·42	0·27
Si	3·00	3·00	3·00	3·00
Al	2·92	3·03	2·95	2·99
Ca	2·06	1·97	1·97	2·02
Ti	<0·01	n.d.	n.d.	n.d.
Σ	7·98	7·99	7·92	8·02

Formulae normalized to 3 Si; n.d., not detected. 1, F-bearing zoisite from run 247 (anorthite + fluorite + titanite seeds); 2, 3, F-bearing zoisites from runs 246 and 228 (anorthite + fluorite); 4, F-bearing zoisite from run 232 (anorthite + kyanite + fluorite + titanite).

With the exception of the natural fluorite, each starting phase was fired at 950°C, and standard drying measures were applied to the capsules before welding. Nevertheless, it is possible that these treatments do not fully dehydroxylate surfaces of finely ground starting materials. After individual phases are fired at high temperature, water could be adsorbed from the atmosphere despite storage in evacuated bell jars. Drying of the weighed charge before welding may not completely dehydrate mineral surfaces. Given the small quantities of F-zoisite ($\ll 1\%$), the charges contain less than $\sim 0{\cdot}0005$ mg of H_2O. As zoisite contains relatively small quantities of H_2O for a hydrous mineral, it will form in comparatively higher—that is, noticeable—modal abundances in the presence of only minor H_2O contamination.

A final mechanism for forming hydrous phases is diffusion of H–O species across the capsule walls. Our experiments were not externally buffered with respect to the fugacities of these components. (One experiment, run 246, was conducted in a sealed gold capsule with a magnetite–hematite buffer to minimize hydrogen diffusion into the capsule; F-zoisite still grew.) Recent studies have demonstrated H_2O loss from hydrous melting experiments in Au or AgPd alloys, implying that this molecule migrates through noble metals (Patiño-Douce & Beard, 1994; Truckenbrodt & Johannes, 1999).

All experiments contain quartz as a run product. This could be due to small amounts of quartz in the synthetic anorthite and titanite. Another possibility could be the formation of quartz through H_2O-involving reactions. The presence of H_2O either through moisture in the air or fluid inclusions in the natural fluorite allows F_2-producing reactions such as reaction (7) to proceed. The initial fO_2 of the capsules is high because of the minor Fe_2O_3 in the natural kyanite and a small amount of O_2-bearing air included during welding. Equilibration at high fO_2 could yield quartz by a reaction such as

$$CaTiSiO_4O + 0{\cdot}5Al_2SiO_5 + 0{\cdot}5F_2 + 0{\cdot}5O_2 = CaAlSiO_4F + TiO_2 + 0{\cdot}5SiO_2 \quad (10)$$

Titanite + Kyanite + Fluid = F–Al-Titanite + Rutile + Quartz.

Reaction (10) might occur in the experiments with mixes F and G (titanite + kyanite + rutile + fluorite) and could be responsible for the formation of quartz and rutile inclusions in newly formed F–Al-titanites.

From the discussion above we conclude that the production of F-bearing zoisite and quartz is readily explained in light of the potential sources of H–O species in the experiments. As F-zoisite is evidently hydrous, whereas F–Al-titanite is not, we infer that zoisite is stabilized by the unanticipated presence of H–O species. However, the low modal proportion of this phase indicates that the concentration of H_2O was low.

Activity–composition relations in titanite solid solutions

The activity of a species in a given phase can be obtained from the displacement of an end-member reaction curve by dilution of one or more participating phases (Wood & Fraser, 1977; Schmid *et al.*, 1978; Wood, 1988). In this study, titanite was diluted with the (Al + F) titanite component, which shifted the position of reaction (5) to lower pressures by about 0·4 GPa at 1000°C and 1100°C. If the experiments are carried out at constant temperature, the activity of $CaTiSiO_4O$ in (Al + F) titanite can be obtained from the relations

$$\int \Delta V_r dP = -RT\ln K \quad (11)$$

where

$$K = a_{CaTiSiO_4O} a_{Al_2SiO_5} / a_{CaAl_2Si_2O_8} a_{TiO_2} \quad (12)$$

and where ΔV_r is the average volume change of reaction (5) between the conditions of the end-member curve and our brackets. The activities of Al_2SiO_5 in kyanite and $CaAl_2Si_2O_8$ in anorthite were approximated with ideal ionic models, and are so close to ideal (0·994–0·998) that within error they are unity. As no analytical data for rutile were available, the activity of TiO_2 in rutile was also assumed to be unity, consistent with the low Al

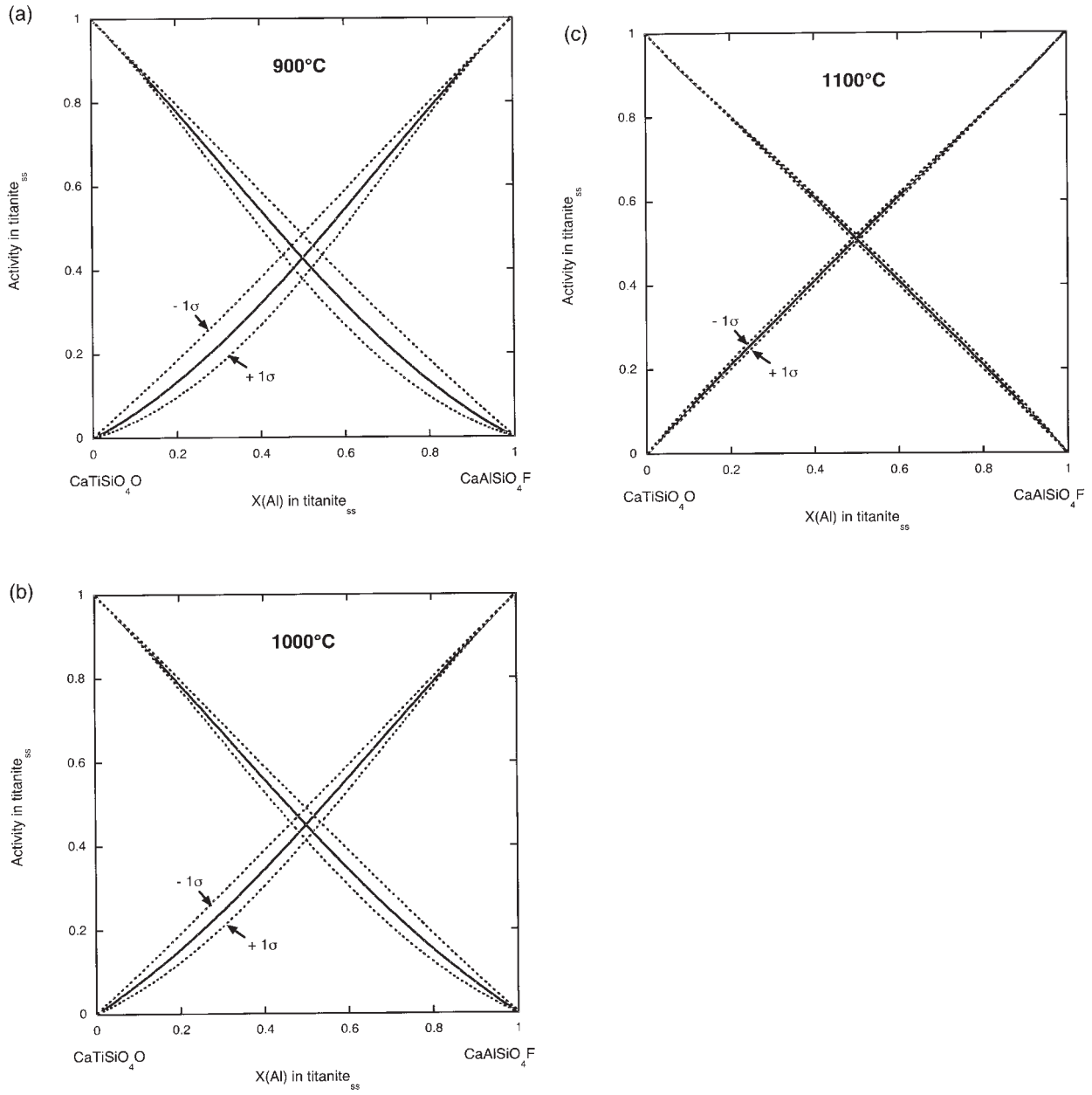

Fig. 12. Activity–composition relationship in (Al + F)-bearing titanites at 900°C (a), 1000°C (b) and 1100°C (c) based on the regular mixing model derived in this study. The continuous line indicates the activity values and the dashed lines show the 1σ standard deviation.

contents (X_{Ti} = 0·98) observed by Manning & Bohlen (1991). Based on these assumptions, equation (12) reduces to

$$K = a_{CaTiSiO_4O}. \quad (13)$$

Assuming the volume change is constant over this pressure interval (0·450 GPa at 900°C, 0·465 GPa at 1000°C and 0·405 GPa at 1100°C) and that the volume relations in the $CaTiSiO_4O$–$CaAlSiO_4F$ solid solution are linear, equations (11) and (12) can be combined to give

$$a_{CaTiSiO_4O} = \exp\left[-\Delta V_r (P_{Exp} - P^0)/RT\right] \quad (14)$$

where P_{Exp} is the pressure of the midpoint of the reversal of this study, involving the solid solution in titanite, and P^0 is the pressure of the calculated end-member curve from the dataset of Holland & Powell (1998).

Solution of equation (14) yields the activity of $CaTiSiO_4O$ in (Al + F) titanite solid solutions of 0·42 ± 0·04, 0·48 ± 0·02 and 0·52 ± 0·02 at 900°C, 1000°C and 1100°C, respectively. The uncertainties are 1σ,

arising from the width of the experimental brackets, but are probably underestimated because of the assumptions outlined above. These data indicate that the activity decreases with falling temperature. The activities from this temperature range are also similar to the activities from the mole fractions of Ti (X_{Ti}) of 0·49 ± 0·04 at 900°C, 0·49 ± 0·03 at 1000°C and 0·51 ± 0·01 at 1100°C; the activity coefficient of $CaTiSiO_4O$ in titanite, $\gamma_{CaTiSiO_4O}$, can be calculated from the relation

$$\gamma_{CaTiSiO_4O} = a_{CaTiSiO_4O}/X_{Ti}. \quad (15)$$

The resulting activity coefficients are 0·87 ± 0·11 at 900°C, 0·91 ± 0·07 at 1000°C and 1·02 ± 0·04 at 1100°C. At the 1σ level, this shows nearly ideal mixing at 1100°C and a negative deviation at 1000°C and 900°C.

A simple symmetric mixing model permits calculation of the interaction parameter, *W*, by using the following expression for the activity coefficient:

$$RT \ln \gamma_{CaTiSiO_4O} = W(X_{1-Ti})^2. \quad (16)$$

This yields a *W* of −6·1 ± 4·9 kJ/mol at 900°C, −0·78 ± 3·1 kJ/mol at 1000°C and 0·93 ± 0·86 kJ/mol at 1100°C for the calculations based on the midpoint of the brackets. Because of the large uncertainty in X_{Ti} and hence the activity coefficients, the resulting 1σ uncertainties in the interaction parameters are too large to be meaningful. Despite these difficulties, we performed a linear regression of the *W* parameter to obtain the temperature dependence of the regular activity model. Fitting the *W* values at 900, 1000 and 1100°C yields $W = -47672 + 34{\cdot}956T$ ($R^2 = 0{\cdot}92$). This allows the calculation of a preliminary regular activity model, which will be used in the calculations discussed below for comparison.

The activity–composition relations at 900°C, 1000°C and 1100°C are shown in Fig. 12a–c. As the data at 900°C have the largest relative uncertainties more experiments are needed to better constrain the activity–composition relationships at lower temperatures. Our results at temperatures above 900°C show that $\gamma_{CaTiSiO_4O} \approx 1$ at high *T*, which suggests that a molecular model is preferable to an ionic model for thermobarometric calculations at high *T*. The obtained data for the regular activity model were taken to calculate the activities of $CaTiSiO_4O$ and $CaAlSiO_4F$ over a temperature range of 500–1100°C (Fig. 13). The activity of $CaTiSiO_4O$ in titanite at temperatures above 1000°C is substantially underestimated by the ionic model used by Manning & Bohlen (1991), in which $a_{CaTiSiO_4O} = X_{Ca}X_{Ti}X_{Si}X_O$[5]. This model assumes independent mixing of Al for Ti and random mixing of F and O on all O sites. However, according to Oberti *et al.* (1991), F substitutes only in one O site (O1) and a fully ionic model should therefore be recast as $a_{CaTiSiO_4O} = X_{Ca}X_{Ti}X_{Si}X_O$, where X_O indicates the mole fraction of O on the (O1) site. As the substitution of F on the (O1) site is coupled with Al, this model is called the ideal coupled model. Figure 13 shows that this ionic model displays a strong negative deviation, which is supported by the results from the experiments at 900°C and the calculated activities at low temperatures. The data suggest that the ideal molecular model (X_{Ti}) should be used at low X_{Al} (<0·2) as the deviation from ideality is still relatively low. At high X_{Al}, the ideal ionic model better predicts the activities at low temperatures, whereas the ideal molecular model is better at high temperatures (>800°C).

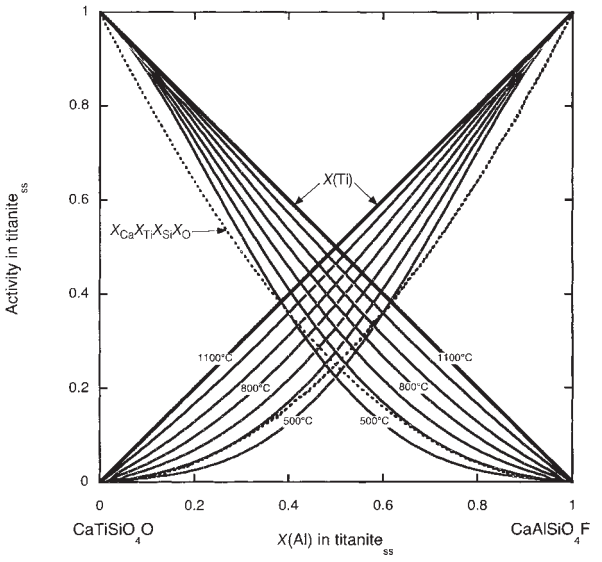

Fig. 13. Comparison between the calculated activities based on the regular activity model from 500°C to 1100°C (continuous lines, this study), the ideal molecular model (X_{Ti}) and the ideal coupled model ($X_{Ca}X_{Ti}X_{Si}X_O$, dashed line).

Our new results can be used to improve pressure estimates for titanite + rutile-bearing eclogites. Manning & Bohlen (1991) experimentally calibrated the end-member reaction (5) and applied it to rocks from various high- and ultra-high-pressure terranes. The results of their calculations, based on the database of Berman (1988), and our study are shown in Table 6. Our calculations were performed with the updated (1998) version THERMOCALC v. 2.7 and the garnet activity model of Ganguly *et al.* (1996). Application of reaction (2) to kyanite-bearing eclogites from Glenelg in Scotland permitted Manning & Bohlen (1991) to calculate equilibration conditions of 1·57–1·60 GPa at 750–760°C. Our recalculations with the ionic model yield 1·66–1·68 GPa and 750–760°C. Applying the molecular activity model (X_{Ti} in titanite) yields slightly higher titanite activities of 0·890, compared with 0·796, based on their ionic activity model. As the change in activity in this case

Table 6: Thermobarometric results

	T (°C)	*P* (GPa) MB (1991)	1σ (GPa)	*P* (GPa) Ionic	1σ (GPa)	*P* (GPa) Molecular	1σ (GPa)	*P* (GPa) Regular	1σ (GPa)
Gleneleg	750–760	1·57–1·60	0·03	1·66–1·68	0·02	1·71–1·73	0·02	1·70–1·73	0·02
Tauern Window	570–650	1·92–2·12	0·12	2·10–2·17	0·11	1·73–1·78	0·12	1·85–1·91	0·10
Kokchetav Massif	830–860	5·62–5·46	0·52	5·82–6·20	0·61	3·31–3·52	0·22	4·03–4·28	0·34

The calculations were performed with the database of Holland & Powell (1998). Ionic refers to the coupled ionic model from the text. Molecular and regular refer to the molecular and regular activity models of titanite discussed in this study. MB (1991) is Manning & Bohlen (1991). The 1σ uncertainties for the MB (1991), ionic and molecular model were calculated according to the error propagation of THERMOCALC v. 2.7 (T. J. B. Holland, personal communication, 1999).

is small it leads to only a negligible shift in pressure of 0·05 GPa to 1·71–1·73 GPa (Table 6). Calculations with the preliminary regular activity model, derived in this study, yield 1·70–1·73 GPa at 750–760°C.

Manning & Bohlen (1991) applied reaction (2) to eclogites from the Eastern Alps, described by Franz & Spear (1985). Recalculation of this reaction with an ionic activity model and THERMOCALC v. 2.7 yields pressures of 2·10–2·17 GPa at 570–650°C, which are slightly higher than in their study. Application of the molecular model for titanite yields pressures of 1·73–1·78 GPa at 570–650°C, about 0·4 GPa lower than their estimates. Using the regular model derived in this study, we obtained pressures of 1·85–1·91 GPa (Table 6).

Finally, Manning & Bohlen (1991) applied titanite-involving reactions to diamond-bearing crustal eclogites from the Kokchetav Massif in Kazakhstan (Sobolev & Shatsky, 1991). Reaction (1) yielded pressures between 4·50 and 4·65 GPa at temperatures of 830–860°C for a $CaTiSiO_4O$ activity of 0·32 in their study. Recalculating this reaction with THERMOCALC v. 2.7 and an ionic model ($CaTiSiO_4O$ activity of 0·31) yields pressures between 5·82 and 6·20 GPa in the same temperature range, more than 1·0 GPa higher than their results. Recalculating the activity of titanite with the molecular activity model yields a $CaTiSiO_4F$ activity of 0·532 and shifts the reaction down to 3·31–3·52 GPa; more than 2 GPa less, whereas application of the regular model yields 4·03–4·28 GPa at 830–860°C. The highly variable results clearly emphasize the importance of the choice of an activity model for more substituted titanites, as a result of the strong negative deviation in the ionic activity model at X_{Al} >0·2 (Table 6).

Derivation of the Gibbs free energy of formation ($\Delta G^\circ_{f,298\cdot15}$) of $CaAlSiO_4F$

Based on the experimental constraints on the displacement of reaction (5) at 1·15 ± 0·05 at 900°C, 1·375 ± 0·025 GPa at 1000°C and 1·575 ± 0·025 GPa at 1100°C, it is possible to calculate $\Delta G^\circ_{f,298\cdot15}$ of $CaAlSiO_4F$. The calculations were performed in two steps, which are outlined below.

Calculation of the end-member curve

The position of the end-member curve of reaction (3), corrected for solid solutions in the participating phases, was calculated by using the experimental reversal brackets of this study at 1000°C and 1100°C. The calculation was performed with available volume, compressibility and expansivity data of the participating phases (Table 4) and the calculated activitiy of $CaAlSiO_4F$ by using the relations

$$\Delta G^\circ_r(P_1, T_1) - \Delta G_r(P_1, T_1) = -RT\ln K. \quad (17)$$

The $\Delta G_r(P_1, T_1)$ represents the free energy change of the reaction at the reversal, involving the solid solutions, and is zero at equilibrium, and $\Delta G^\circ_r(P_1, T_1)$ is the free energy change of the reaction involving pure end-member phases. The free energy change ΔG° for the end-member curve between the reversal (P_1, T_1) and its theoretical position in P–T space (P_2, T_1) is obtained by

$$\Delta G^\circ_r(P_2, T_1) - \Delta G^\circ_r(P_1, T_1) = \int \Delta V\, dP. \quad (18)$$

As the free energy change is zero at equilibrium, equation (18) yields

$$\Delta G^\circ_r(P_2, T_1) = \int \Delta V\, dP + RT\ln K. \quad (19)$$

The calculated position of the end-member curve of reaction (3) lies at 2·06 GPa at 1000°C and 2·29 GPa at 1100°C.

Calculation of the free energy of formation ($\Delta G^\circ_{f,298\cdot15}$) of $CaAlSiO_4F$

Starting with the conditions of the pure end-member curve, $\Delta G^\circ_{r,298\cdot15}$ is obtained by solving the relation

Table 7: $S°_{298·15}$ *and* Cp *coefficients used in thermodynamic calculations*

Phase	$S°_{298}$	Ref.	a_1	a_2	a_3 (10^6)	a_4 (10^3)	a_5 (10^{-9})	Ref.
Anorthite	200·0	(2)	371·60	0·013	−4·11	−2·04	0·423	(2)
FAT	105·2	(1)	423·42	−0·085	1·24	−4·79	9852·0	(1)
Forsterite	94·1	(2)	87·36	0·087	−3·70	0·84	22370·0	(3)
Monticellite	108·1	(2)	231·40	−0·001	−1·25	−1·62	1·333	(3)
F-topaz	105·4	(2)	471·40	−0·082	1·27	−5·49	0·00	(3)
Fluorite	68·9	(3)	2033	−1·436	29·88	−33·12	50402·0	(3)

$S°_{298·15}$ in J/bar K; $Cp = a_1 + a_2T + a_3(T^{-2}) + a_4(T^{-0·5}) + a_5(T^2)$. Ref. (reference): (1) this study; (2) Holland & Powell (1998); (3) Robie & Hemingway (1995).

Table 8: $\Delta G°_{f,298·15}$ *and* $\Delta H°_{f,298·15}$ *of* $CaAlSiO_4F$ *from this study*

	$S°_{298·15}$ = 105·2 J/mol K			$S°_{298·15}$ = 109·6 J/mol K		
T (°C):	900°C	1000°C	1100°C	900°C	1000°C	1100°C
$\Delta G°_{f,298·15}$	−2596 ± 1	−2597 ± 0·5	−2598 ± 0·4	−2592 ± 1	−2593 ± 0·5	−2593 ± 0·4
$\Delta H°_{f,298·15}$	−2745 ± 1	−2746 ± 0·5	−2747 ± 0·4	−2741 ± 1	−2742 ± 0·5	−2742 ± 0·4

The $\Delta G°_{f,298·15}$ and $\Delta H°_{f,298·15}$ values are in kJ/mol; the 1σ uncertainty is based on the uncertainty in the obtained activities.

$$\Delta G°_r(P_1, T_{298·15}) - \Delta G°_r(P_2, T_2) = \int \Delta V \, dP - \int \Delta S \, dT. \quad (20)$$

$\Delta G°_r(P_1, T_{298·15})$ is the free energy change of reaction (4) at 1 bar and 298·15 K, and $\Delta G°_r(P_2, T_2)$ is the free energy change at the conditions of the pure end-member curve and is zero. For these calculations we use the data of Holland & Powell (1998) for anorthite, Robie & Hemingway (1995) for fluorite and our own $S°_{298·15}$ estimates for FAT. The heat capacity (Cp) was estimated based on an additive scheme of reaction (6) and is shown in Table 7. Calculation of $\Delta G°_r(P_1, T_{298·15})$ with $S°_{298·15}$ estimates for $CaAlSiO_4F$ of 105·2 J/mol K and 109·6 J/mol K yields values ranging between 8·7–13·5 and 1·03–4·04 kJ/mol. The $\Delta G°_{f,298·15}$ of $CaAlSiO_4F$ is obtained by

$$\Delta G°_{f,FAT} = [\Delta G°_{f,An} + \Delta G°_{f,Fl} - \Delta G°_r(P_1, T_{298·15})]/2. \quad (21)$$

The value for $\Delta G_{f,Fl}$ was taken from Robie & Hemingway (1995), yielding standard free energies of formation of $CaAlSiO_4F$ of −2597 ± 0·5 and −2593 ± 0·5 kJ/mol using the 1000°C bracket and −2598 ± 0·4 and −2593 ± 0·4 kJ/mol using the 1100°C bracket (Table 8). For comparison, $\Delta G°_f$ of titanite is −2454·60 kJ/mol (Holland & Powell, 1998). The standard enthalpy of formation $\Delta H°_{f,FAT}$ can be calculated by using the relation

$$\Delta H°_{f,FAT} = \Delta G°_{f,FAT} + T\Delta S°_{FAT} \quad (22)$$

where $\Delta S°_{f,FAT}$ stands for

$$\Delta S°_{FAT} = \Delta S°_{FAT} - \Sigma S°_{Elements}. \quad (23)$$

The entropy of the elements was taken from Robie & Hemingway (1995) and $S°_{FAT}$ at 298·15 K was taken from the estimation above. This yields $\Delta H°_{f,298·15}$ of $CaAlSiO_4F$ ranging from −2741 ± 1 to −2747 ± 0·4 kJ/mol (Table 8). Based on these calculations, it is possible to calculate the position of the AFT reaction (3) in *P–T* space. This is shown in Fig. 14. The intersection of reaction (3) and reaction (5) is at 400°C and 0·5 GPa, if the calculations are performed with $S°_{FAT}$ of 105·2 J/mol K. If an $S°_{FAT}$ of 109·6 J/mol K is chosen the intersection occurs at negative temperatures. This shows the crucial role of a firm constraint on $S°_{FAT}$ for future phase equilibrium calculations involving $CaAlSiO_4F$.

CONCLUSIONS

Figures 5–11 illustrate the relative roles of *P*, *T* and buffering assemblage on titanite composition. Titanite

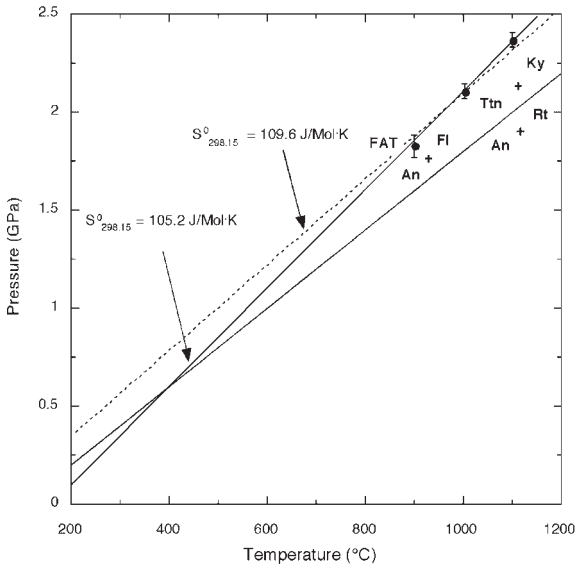

Fig. 14. The calculated positions of reactions (3) (AFT) and (5) (TARK). The continuous line shows the position of reaction (3) when calculated with $S°_{298·15}$ of $CaAlSiO_4F$ of 105·2 J/mol K, and the dashed line shows the position when calculated with $S°_{298·15}$ = 109·6 J/mol K.

compositions are potentially useful recorders of P or T, independent of bulk composition, when they are part of appropriate mineral assemblages. The maximum change in titanite composition with P and T occurs in the presence of anorthite and fluorite (AFT). The assemblage titanite + anorthite + Al_2SiO_5 + rutile (TARK) produces titanite compositions at low X_{Al}, with the maximum X_{Al} being controlled by the isothermally or isobarically invariant point. Titanite compositions in equilibrium with both these assemblages are sensitive functions of P and T. By contrast, when titanite coexists with rutile, fluorite and Al_2SiO_5 (TAFT), its composition does not change significantly with P and T, because of the steep P–X_{Al} and T–X_{Al} slope of this univariant line.

The results of this study show that the critical issue governing the F–Al content of titanite solid solutions is the coexisting assemblage. Many natural assemblages have a higher number of chemical components than number of phases and are therefore unbuffered with regard to a chemical variable (e.g. Al content of titanite). The Al content is therefore not merely a function of P and T, but of the bulk composition of the rocks. Important compositional variables will be those that control the An content of the plagioclase or the clinozoisite content of epidote, etc., which will have an influence on the reaction progress of reactions such as (3) in P–T space.

The reaction displacement experiments show that at high pressures the assemblage (Al + F) titanite + kyanite + rutile + fluorite is stable and at low pressures the assemblage (Al + F) titanite + anorthite + rutile + fluorite is stable. The data show that the activity is very close to the ideal molecular activity model (X_{Ti}) at 1100°C, but show a negative deviation at 1000°C and 900°C. As the chemical data at 900°C and 1000°C show large uncertainties, owing to chemical heterogeneities in the experiments, the molecular activity model as an approximation is recommended for use in calculations for titanites with X_{Al} = 0·1–0·4, until more data are available. Although our data were obtained at high temperatures (900–1100°C), they provide important constraints on a possible activity model. The current data do *not* allow the extraction of meaningful values of the interaction parameter, W, of a regular solid solution model, as a result of the chemical variations of the (Al + F) titanite compositions and the experimental uncertainties. For calculations involving natural (Al + F)-rich titanites in the compositional range of X_{Al} = 0·1–0·3, the molecular model seems to be the better approach to predict the activity of $CaTiSiO_4O$ in titanite than the ionic models at high temperatures. Recalculation of the P–T conditions of three eclogites illustrates the difference in pressure estimates resulting from the choice of different activity models (molecular vs ionic) ranging from 0·05 to 2·1 GPa, depending on the $CaAlSiO_4F$ substitution in the natural titanites and the sensitivity of reactions to changes in the activity of $CaTiSiO_4O$ in titanite.

Troitzsch & Ellis (2002) recently published a study on the thermodynamic properties of F–Al-titanite. Based on displacement of the reaction (AFT) anorthite + fluorite = F–Al-titanite, they derived a $\Delta H°_{f,FAT}$ of −2740·8 ± 3 kJ/mol, which is in good agreement with the results of our study, −2744 ± 3 kJ/mol. Our entropy estimates for $S°_{FAT}$ range from 105·2 to 109·6 J/mol K, which is also in agreement with their estimated entropy of 104·9 ± 1·1 J/mol K. The two studies differ only in: (1) the choice of the activity model and the estimated values of the interaction parameter W for the solid solution; (2) the experimental approach to determine the shift of the AFT reaction. In our calculations we used a simple symmetrical model, which resulted in a negative deviation from ideality, in contrast to the slight positive deviation in their local balance and multi-site mixing models. The data for W obtained in our study are directly based on experiments and have definitive negative deviations. Troitzsch & Ellis measured the pressure and temperature dependence of X_{Al} in titanite in the assemblage F–Al-titanite + anorthite + fluorite and then calculated the position of the end-member AFT reaction based on the two activity models, a multi-site mixing model and a local charge balance model. In our study, we determined the shift of the reversals of the TARK reaction anorthite + rutile = titanite and kyanite in the presence of fluorite. Based on these reversals we then calculated the end-member position of the AFT reaction over a temperature range of 900–1100°C. Our results show a very good agreement with their calculated end-member position

based on a local charge balance model, whereas their multi-site mixing model overestimates the pressures of the position of AFT at 1000°C and 1100°C by 0·1–0·2 GPa.

The variation in $\Delta G°_{f,FAT}$ and $\Delta H°_{f,FAT}$ of nearly 6 kJ/mol in our study and up to 10 kJ/mol by comparing our data with those of Troitzsch & Ellis (2002) mainly results from the different entropy estimates for $CaAlSiO_4F$ applied in the calculations. Until more reliable entropy estimates from calorimetric measurements are available, these obtained values of $\Delta G°_{f,FAT}$ and $\Delta H°_{f,FAT}$ are only of preliminary nature.

ACKNOWLEDGEMENTS

This work was supported by NSF grants EAR 95-26596 and EAR 92-05649 to E.J.E. and EAR 94-05999 and EAR 99-09583 to C.E.M., a fellowship from the Austrian Bundesministerium für Wissenschaft und Forschung, and grants from the International Institute of the University of Michigan, Turner Fund of the Department of Geological Sciences at the University of Michigan, and the Geological Society of America to P.T. Heather Lin, Tom LaTourette, Robert Newton and Kurt Knesel are thanked for their help in the UCLA piston–cylinder laboratory, and Wayne Dollase for his help with the X-ray diffractometer. The comments of John Ferry on an earlier draft of the manuscript are gratefully acknowledged. The journal reviews of Paul Hoskin and Gregor Markl and the editorial handling of Kurt Bucher are also gratefully acknowledged. Carl Henderson is thanked for his assistance with the EMP at the Electron Microbeam Analysis Laboratory (EMAL) at the University of Michigan, and Frank Kyte and Patricia Weston for their assistance with the EMP at UCLA. Karl Ettinger is thanked for his help with the scanning electron microscope at the Institute of Mineralogy and Petrology, University of Graz. This is Publication Number 517 of the Mineralogical Laboratory of the University of Michigan.

REFERENCES

Berman, R. G. (1988). Internally-consistent thermodynamic data for minerals in the system Na_2O–K_2O–CaO–FeO–Fe_2O_3–Al_2O_3–SiO_2–TiO_2–H_2O–CO_2. *Journal of Petrology* **29**, 445–522.

Bernau, R., Franz, G. & Langer, K. (1986). Experimental investigation of titanite in the system CaO–Al_2O_3–TiO_2–SiO_2–H_2O. *Experimental Mineralogy and Geochemistry International Symposium, Nancy (France), Abstracts*, 21–22.

Boettcher, A. L., Windom, K. E., Bohlen, S. R. & Luth, R. W. (1981). Low-friction, anhydrous, low- to high-temperature furnace assembly for piston–cylinder apparatus. *Reviews of Scientific Instruments* **52**, 1903–1904.

Bohlen, S. R. (1984). Equilibria for precise pressure calibration and a frictionless furnace assembly for the piston–cylinder apparatus. *Neues Jahrbuch für Mineralogie, Monatshefte* **9**, 404–412.

Bohlen, S. R., Montana, A. L. & Kerrick, D. M. (1991). Precise determination of the equilibria kyanite–sillimanite and kyanite–andalusite and a revised triple point for Al_2SiO_5 polymorphs. *American Mineralogist* **76**, 677–680.

Boyd, F. R. & England, J. L. (1960). Apparatus for phase equilibrium measurements at pressures up to 50 kilobars and temperatures up to 1750°C. *Journal of Geophysical Research* **65**, 741–748.

Carswell, D. A., Wilson, R. N. & Zhai, M. (1996). Ultra-high pressure aluminous titanites in carbonate-bearing eclogites at Shuanghe in Dabieshan, central China. *Mineralogical Magazine* **60**, 461–471.

Enami, M., Suzuki, K., Liou, J. G. & Bird, D. K. (1993). Al–Fe^{3+} and F–OH substitutions in titanite and constraints on their *P*–*T* dependence. *European Journal of Mineralogy* **5**, 219–231.

Fehr, K. T. (1991). Al–OH Einbau in Titanit: ein neues Geothermobarometer. *Beihefte zum European Journal of Mineralogy* **3**, 76.

Franz, G. & Spear, F. S. (1985). Aluminous titanite (titanite) from the eclogite zone, south central Tauern window, Austria. *Chemical Geology* **50**, 33–46.

Ganguly, J., Weiji, C. & Tirone, M. (1996). Thermodynamics of aluminosilicate garnet solid solution: new experimental data, an optimized model and thermometric applications. *Contributions to Mineralogy and Petrology* **126**, 137–151.

Gibert, F., Moine, B. & Gibert, B. (1990). Titanites (sphenes) alumineuses formées a basse/moyenne pression dans la gneiss à silicates calciques de la Montagne Noire. *Comptes Rendus de l'Académie des Sciences, Série II* **311**, 657–663.

Higgins, J. B. & Ribbe, P. H. (1976). The crystal chemistry and space groups of natural and synthetic titanites. *American Mineralogist* **61**, 878–888.

Hollabaugh, C. L. (1980). Experimental mineralogy and crystal chemistry of sphene in the system soda–lime–alumina–titania–silica–water. Ph.D. thesis, Washington State University, Pullman, 116 pp.

Holland, T. J. B. (1989). Dependence of entropy on volume for silicate and oxide minerals: a review and a predictive model. *American Mineralogist* **74**, 5–13.

Holland, T. J. B. & Powell, R. (1998) An internally-consistent thermodynamic data set for phases of petrological interest. *Journal of Metamorphic Geology* **8**, 89–124.

Johannes, W., Chipman, D. W., Hays, J. F., Bell, P. M., Mao, H. K., Newton, R. C., Boettcher, A. L. & Seifert, F. (1971). An interlaboratory comparison of piston–cylinder pressure calibration using the albite-breakdown reaction. *Contributions to Mineralogy and Petrology* **32**, 24–38.

Kretz, R. (1983). Symbols for rock-forming minerals. *American Mineralogist* **68**, 277–279.

Leinenweber, K., Grzechnik, A., Voorhees, M., Navrotsky, A., Yao, A. & McMillan, P. F. (1997). Structural variation in $Ca(Ti_xSi_{1-x})O_3$ perovskites and the ordered phase Ca_2TiSiO_6. *Physics and Chemistry of Minerals* **24**, 528–534.

Manning, C. E. & Bird, D. K. (1990). Fluorian garnets from the host rocks of the Skaergaard intrusion: implications for metamorphic fluid composition. *American Mineralogist* **75**, 859–873.

Manning, C. E. & Boettcher, S. L. (1994). Rapid-quench hydrothermal experiments at mantle pressures and temperatures. *American Mineralogist* **79**, 1153–1158.

Manning, C. E. & Bohlen, S. R. (1991). The reaction titanite + kyanite = anorthite + rutile and titanite–rutile barometry in eclogites. *Contributions to Mineralogy and Petrology* **109**, 1–9.

Markl, G. & Piazolo, S. (1999). Stability of high-Al titanite from low-pressure calcsilicates in light of fluid and host-rock composition. *American Mineralogist* **84**, 37–47.

McNear, E., Vincent, M. G. & Parthe, E. (1976). The crystal structure of vuagnatite $CaAlSiO_4(OH)$. *American Mineralogist* **61**, 831–838.

Oberti, R., Smith, D. C., Rossi, G. & Caucia, F. (1991). The crystal chemistry of high-aluminum titanites. *European Journal of Mineralogy* **3**, 777–792.

Patiño-Douce, A. E. & Beard, J. S. (1994). H_2O loss from hydrous melts during fluid-absent piston cylinder experiments. *American Mineralogist* **79**, 585–588.

Ribbe, P. H. (1982). Titanite. In: Ribbe, P. H. (ed.) *Orthosilicates. Mineralogical Society of America, Reviews in Mineralogy* **5**, 137–155.

Robie, R. & Hemingway, B. (1995). Thermodynamic properties of minerals and related substances at 298·15 K and 1 bar (10^5 Pascals) pressure and higher temperatures. *US Geological Survey Bulletin* **2131**, 461 pp.

Robinson, G. R. & Haas, J. L. (1983). Heat capacity, relative enthalpy, and calorimetric entropy of silicate minerals: an empirical method of prediction. *American Mineralogist* **68**, 541–553.

Schmid, R., Cressey, G. & Wood, B. J. (1978). Experimental determination of univariant equilibria using divariant solid solution assemblages. *American Mineralogist* **63**, 511–515.

Smith, D. C. (1977). Aluminium bearing sphene in eclogites from Sunnmore (Norway). *Geolognytt* **10**, 32–33.

Smith, D. C. (1981). The pressure and temperature dependence of Al-solubility in titanite in the system Ti–Al–Ca–Si–O–F. *Progress in Experimental Petrology, NERC Publication Series D* **18**, 193–197.

Sobolev, N. V. & Shatsky, V. S. (1991). Diamond inclusions in garnets from metamorphic rocks: a new environment for diamond formation. *Nature* **343**, 742–746.

Troitzsch, U. & Ellis, D. J. (1999). The synthesis and crystal structure of $CaAlFSiO_4$, the Al–F analog of titanite. *American Mineralogist* **84**, 1162–1169.

Troitzsch, U. & Ellis, D. J. (2002). Thermodynamic properties and stability of AlF-bearing titanite $CaTiOSiO_4$–$CaAlFSiO_4$. *Contributions to Mineralogy and Petrology* **142**, 543–563.

Tropper, P. (1998). Experimental and field-related investigations on the metamorphic history of the Sesia–Lanzo Zone (Western Alps, Italy). Ph.D. thesis, University of Michigan, Ann Arbor, 258 pp.

Truckenbrodt, J. & Johannes, W. (1999). H_2O loss during piston–cylinder experiments. *American Mineralogist* **84**, 1333–1335.

Vaidya, S. N., Bailey, S., Pasternack, T. & Kennedy, G. C. (1973). Compressibility of fifteen minerals to 45 kbars. *Journal of Geophysical Research* **78**, 6893–6898.

Valley, J. W., Essene, E. J. & Peacor, D. R. (1983). Fluorine-bearing garnets in Adirondack calc-silicates. *American Mineralogist* **68**, 444–448.

Wood, B. J. (1988). Activity measurements and excess entropy–volume relationships for pyrope–grossular garnets. *Journal of Geology* **96**, 721–729.

Wood, B. J. & Fraser, D. G. (1977). *Elementary Thermodynamics for Geologists*. Oxford: Oxford University Press, 303 pp.

Xirouchakis, D. & Lindsley, D. H. (1998). Equilibria among titanite, hedenbergite, fayalite, quartz, ilmenite and magnetite: experiments and internally consistent thermodynamic data for titanite. *American Mineralogist* **83**, 712–725.